Design of Tapered and Straight Stator Pole Switched Reluctance Machines

Lizo M.M. Sitsha

Thesis presented in partial fulfilment of the requirements for the degree of Master of Science in Electrical Engineering at the University of Stellenbosch

Supervisor: Dr. M.J. Kamper

March 2000

Declaration

I, the undersigned, hereby declare that the work contained in this thesis is my own original work and that I have not previously in its entirety or in part submitted it at any university for a degree.

Abstract

This thesis deals with the design and optimisation of medium power traction switched reluctance machines with tapered and straight stator poles. Only the prototype of the tapered stator pole machine is constructed and evaluated in this study.

A non-commercial finite element package is used in the design and optimisation of the machines. The finite element method is applied directly in the optimisation procedure to optimise the design of the machines in multi-dimensions. The lumped circuit analysis method is used only for the purpose of verifying some of the finite element calculated. It is not used in the optimisation procedure.

The performance characteristics of the tapered and straight stator pole machines are compared and discussed and the tapered stator pole machine is found to have better torque performance. Also the calculated and measured static torque versus rotor position characteristics of the tapered stator pole machine are compared and discussed.

Opsomming

Die tesis beskryf die ontwerp en optimering van medium drywing trekkrag geskakelde reluktansie masjiene met tapse en reguit stator pole. Slegs 'n prototipe van die tapse stator pool masjien is gebou en geëvalueer.

Die masjiene is ontwerp en geoptimeer met behulp van 'n nie-kommersiële eindige element metode pakket. Die eindige element metode is direk in die optimerings algoritme gebruik vir die optimering van die masjiene in multi-dimensies. Die gekonsentreede parameter stroombaananalise is slegs gebruik om sommige van die eindige element berekenings te verifeer.

Die vermoës van die tapse en reguit stator pool masjiene is vergelyk en bespreek. Die resultate toon dat die tapse stator pool masjien se draaimoment vermoë beter is as die van die reguit stator pool masjien. Die berekende en gemete statiese draaimoment teenoor rotorposisie van die tapse stator pool masjien is ook vergelyk en bespreek.

Acknowledgments

I would like to thank my supervisor, Dr. M.J. Kamper, for the constant support and encouragement he gave me throughout the course of my studies. I would also like to acknowledge the following persons for their invaluable contribution to this work and without whom the completion of this study would not have been possible:

- The technical staff of the electrical workshop.
- Messrs. J. Blom and J. Weerdenburg, who assisted me with all the mechanically related aspects.
- All members of the electrical machines group for their interest and support.
- LIW for their financial support.
- My family and friends for their interest and constant support.
- My baby son, Luvuyo who had to grow up without me during the study period.
- I would also like to thank the Almighty for giving me strength and courage.

Contents

List of Figures

List of Tables

List of Symbols

st_od	stator outer diameter
st_id	stator inner diameter
st_sh	stator slot height
st_pw	stator pole width
st_sw	stator slot width
st_yh	stator yoke height
ro_od	rotor outer diameter
ro_shd	rotor shaft diameter
ro_yh	rotor yoke height
ro_tw	rotor tooth width
sp_tip	stator pole tip
sp_base	stator pole base
g	air-gap length
t_s	stator pole width
λ_s	stator pole pitch
sr	split ratio (st_od/st_id)
t_r	rotor pole width
λ_r	rotor pole pitch
bc	st_yh/st_pw

Chapter 1

Introduction

1.1 History of the SRM and well-known literature

The concept of rotating electrical machines was borne out of the observation that an electromagnetic coil attracts a piece of iron. The force resulting from this attraction could then be used to obtain mechanical motion. The first reluctance motor was built about 160 years ago based on this observation but the motor could not realise its full potential. Until the modern advancements in power electronics the reluctance motor was considered inefficient with low specific power output.

The independent work by Lawrenson and Stephenson of Leeds University and Davis and Ray of Nottingham University brought about the potential these motors can offer in terms of efficiency and cost-effectiveness in comparison to other machines. They combined their development resources in 1975, and their first commercial outcome of their research was the Oulton variable speed drive. At least two authors [14] and [2] give two important developments worth mentioning that made the reluctance motor viable again:

1. The advent of high-power computer has enabled a very detailed analysis of the motor electromagnetic profile to be optimised, eg. the computer aided design (CAD) and finite element method (FEM).

2. The advent of high-power semiconductor switches in the 1960's has raised its performance to greater levels and brought out optimum performance from the motor.

Even to date there is still a growing interest in the Switched Reluctance Motors so that their application is being investigated in various fields by engineers, particularly in the field of traction because of their low weight/torque ratio and high reliability. The Switched Reluctance Motor

(SRM) is characterised by double saliency and unexcited rotor, i.e. the motor has salient poles on both the stator and the rotor and that the rotor has no windings or permanent magnets. This makes the SRM robust and almost maintenance free.

The advantages may be summarised as follows:

- The stator is simple to wind; the end turns are short and robust and have no phase-phase crossovers.
- Although the flux pulsations in the rotor causes rotor iron losses, especially at high speed, most of the cooling of the machine is necessary on the stator, which is relatively easy to cool.
- The rotor is simple and is easy to manufacture; it also tends to have a low inertia.
- Because there are no magnets on the rotor the maximum permissible rotor temperature may be higher than in PM motors.
- The torque is independent of the polarity of phase current and for certain applications this permits a reduction in the number of power semiconductor switches needed in the controller.
- Most converter circuits used for SRMs are immune from shoot-through faults.
- Extremely high speeds are possible.

The major drawbacks of the SRM are the acoustic noise and the tendency of the machine to produce torque with high ripple. The latter may be considered as making the SRM unsuitable for very low speed operations.

1.2 Problem statement

As far as the author is concerned, very little work has been published in literature on tapering the SRM poles. Recent studies conducted by [3] have shown that the stator pole tapering has significant impact on shaping the electromagnetic torque and self-inductances of the machine while the rotor pole tapering has been found to have very little effect. This thesis therefore proposes the tapered stator pole configuration, where almost all of the copper and iron area available on the stator is utilised. The stator pole tapering is also done mainly to optimise the average and peak torque of the machine so that the machine is suitable for traction applications.

It has also been found that in the design optimisation of SRMs the tendency in literature was to optimise only particular variables relevant to the researcher and not the whole machine, an example of this is evident in [3], where on tapering the stator poles the authors only varied the base pole arcs and kept the arc tips constant. In this thesis, both the base pole arc and arc tip must be varied and an attempt to optimise all the variables of the machine must be done.

To do a design optimisation of the SRM, an objective function like the torque of the machine must be maximised subject to constraints, if any. An optimisation algorithm is therefore necessary to optimise in multidimensions the design of the machine [16]. It must be emphasised that all the machine variables must be optimised to put the objective function value at a minimum (maximum). It is not sufficient to focus only on single variables in the design of the machine and to reach certain conclusions from that. All the variables must be looked at in the design optimisation.

The SRMs are known to be highly non-linear and because of this fact it is very difficult to derive and use analytical expressions to predict the machine performances. Although the lumped circuit method can be employed, it will not give the optimum results. The best possible method that can be used to obtain the absolute optimum designed machine is by using the finite element solution directly in the optimisation process.

The problem with the tapered stator pole configuration seems to be the difficulty in manufacturing and fitting of the stator coils into the slots because of the shape of the stator poles, but V-shaped coils could make this task easy, in terms of both manufacturing and fitting.

1.3 Approach to problem

In the design optimisation of the SRM only the static characteristics are considered in this thesis. As mentioned in section 1.2, the approach that is followed in this thesis is to use the finite element method directly in the optimisation procedure. This approach may be best explained with the aid of the flow diagram of Fig. 1.1. Here, the optimisation algorithm finds the multidimensional vector [X], i.e. the values of the machine variables (the machine variables include amongst other things the physical dimensions of the machine) that minimise (or maximise) the function value Y or performance parameter of the machine. In this process with each iteration r the algorithm determines directions of search in a multidimensional space along which Y is minimised (or maximised). Each time the optimisation algorithm needs an output function value Y, like torque or efficiency, for a given multidimensional input vector [X], it calls the finite element program. The finite element program generates a new mesh according to the changed input variables. The program then does the pre-processing and the non-linear solution to find the magnetic vector

potentials. The flux linkages and flux densities are calculated, followed by the calculation of the output performance parameters Y of the machine. The finite element program may be called a number of times by the algorithm during an iteration. At the end of each iteration a test is carried out to determine if an absolute minimum (or maximum) is reached. If not, a next iteration is executed.

It is obvious that the process represented in Fig. 1.1 will be time consuming. This necessitates the following:

- The finite element solution must be fast and accurate, i.e. generating the mesh, doing the pre-processing and solving for the vector potentials must be a fast and accurate process.
- As a few finite element solutions as possible must be used to calculate all the equivalent circuit parameters and performance data of the machine. For example, it will be beneficial if the performance parameters of the machine can be calculated by using the results of one basic set of finite element solutions.
- The optimisation algorithm must be fast.

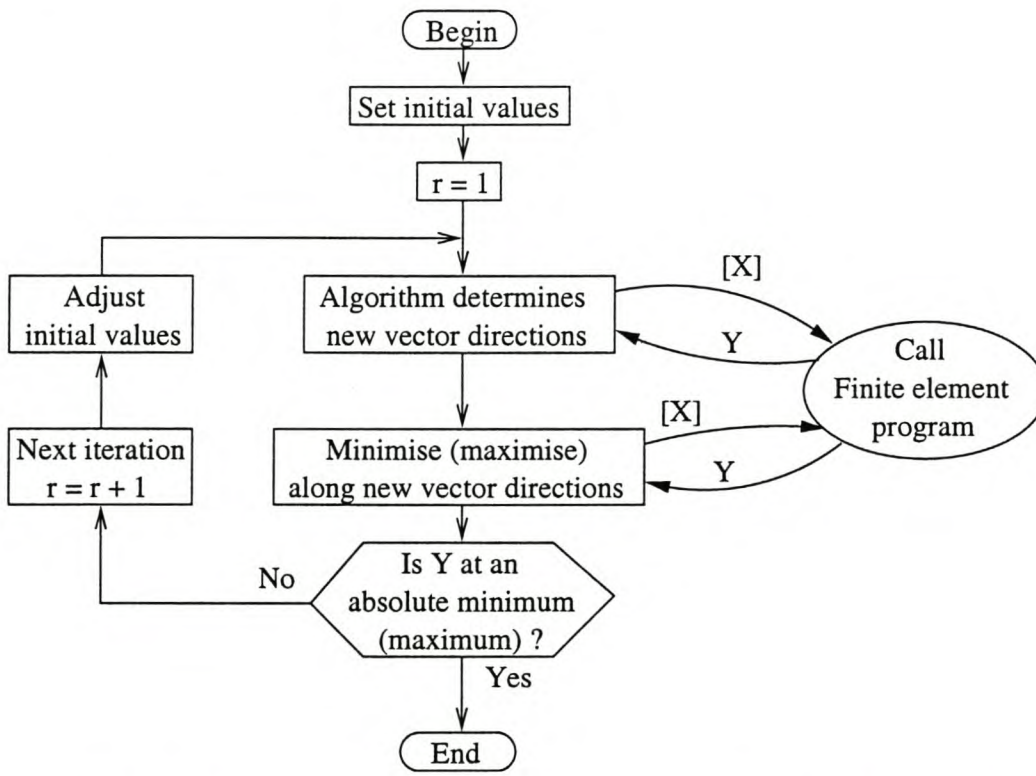

Figure 1.1: **Optimisation procedure using the finite element solution directly [16].**

A non-commercial finite element software package developed at the University of Cambridge is used for this study. The advantage of using the non-commercial package over the commercial one is the availability of the source code which makes it possible to realise the process described by Fig. 1.1. With the source code available it was possible to link the finite element and the optimisation algorithm programs with each other.

1.4 Layout of the thesis

The layout of this thesis is as follows:

Chapter 2: This chapter looks into different SRM design configurations. The static torque production is discussed briefly as well as the voltage equation and energy flow.

Chapter 3: The different most commonly used converter topologies and SRM drives are briefly discussed with their advantages and disadvantages. The chapter also deals with the drive system and operation.

Chapter 4: The focus of this chapter is on the multidimensional optimisation algorithm used to design the SRM. The FEM is briefly discussed here and FEM solution is given for both the tapered stator pole and the straight stator pole machines. The chapter also makes comparison some results of the FEM solution with some results of the lumped circuit analysis.

Chapter 5: This chapter compares the performance characteristics of the tapered stator pole SRM with that of the straight stator pole SRM. In particular, the static torque versus angle characteristics are compared and discussed.

Chapter 6: The test results of the tapered stator pole SRM are compared with simulated results. The layout of the test system is also described briefly.

Chapter 7: In this chapter conclusions are drawn and recommendations are made for further research work.

Chapter 2

Structural considerations and SRM Operation

This chapter briefly discuss the different types of SRM configurations, i.e. different SRMs have different pole shapes, stator-rotor pole ratios or number of teeth per pole, depending on what the machine is designed for. A theoretical account of the inductance variation as a function of rotor position is given and static torque production is also briefly discussed. The voltage equations are also given.

2.1 Machine configuration

SRMs in general have the same basic structure, i.e. they are doubly-salient and have rotors with no conductors or permanent magnets. However, there are many variations of SRMs available, depending on their applications. The major differences are in the pole shapes, stator-rotor pole ratios, the number of teeth per pole and the number of poles per phase. The relationship between number of poles per phase and the number of phases is not fixed but it is common in many applications to associate for a certain stator-rotor pole combination, the number of phases, e.g. the 6:4 and 8:6 pole combinations are always associated with three-phase and four-phase motors, respectively. It should also be noted that SRMs have unequal numbers of salient poles on the stator and the rotor.

2.1.1 Pole shapes

Two types of pole shapes will be dealt with in this thesis, namely (i) Conventional straight poles and, (ii) Tapered poles. The pole shapes refer specifically to the geometry of the stator

poles. The tapered stator pole shape means that the base and the tip of the pole are not of the same width as in straight stator poles. The difference can be seen clearly in Figs. 2.1 and 2.2. According to [3] and [4] only the tapering of the stator poles has a significant influence on the torque characteristics. It can be seen from the figures below that the tapered pole machine utilises almost all of the winding area in the stator slots. It can also be mentioned that although tapered poles have some obvious advantages over the conventional straight poles, they add little extra weight to the machine as compared to the straight poles. For traction purposes weight is very important.

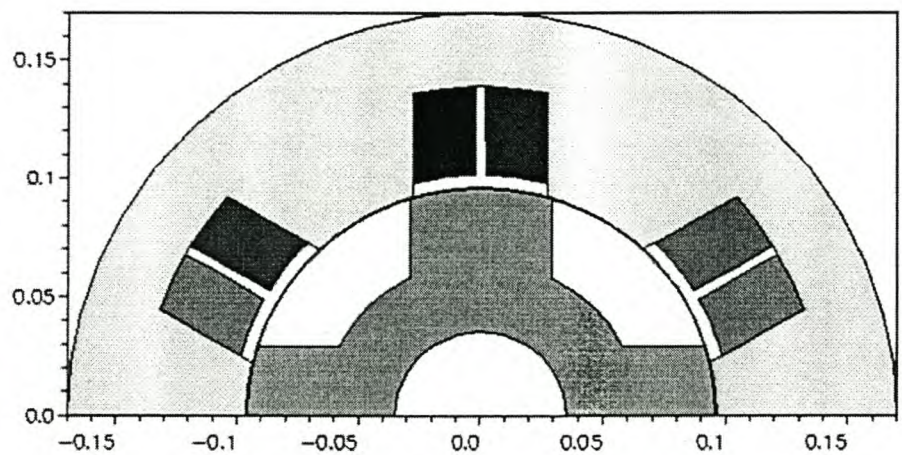

Figure 2.1: **Tapered stator pole SRM**

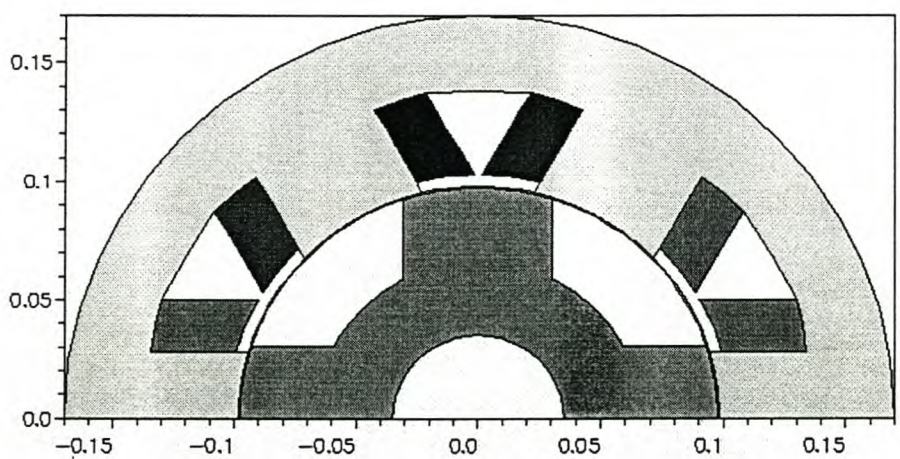

Figure 2.2: **Straight stator pole SRM**

2.1.2 Number of poles and multi-toothed poles

It is known from stepping motor studies that it is desirable, from the point of view of maximising machine output, to eliminate mutual inductance between phases [8]. The study of [8] also states that careful consideration has shown that mutual inductance due to main (airgap) flux will be zero for the following features:

- the iron is infinitely permeable
- the stator poles are excited in diametrically opposite pairs
- the rotor has an even number of poles

It must also be taken into consideration that since the performance of the SRM improves with the ratio $\frac{pole pitch}{air gap} = \frac{\lambda}{g}$, and g depends on mechanical considerations, it is obviously important to have the pole pitch λ as large as possible. The pole pitch can be increased by decreasing the number of poles. In practice, the minimum number of poles for all but very small machines is four. The number of poles must, however, also be evaluated against other considerations, namely:

- more poles reduce torque ripple
- more poles increase exciting frequency (at the same speed) and the associated losses, where the exciting frequency is given by

$$f_s = N_r * \frac{\omega}{2\pi}, \tag{2.1}$$

where N_r is the number of rotor poles and ω is the rotor speed in radians.

The above arguments therefore imply that a large number of poles would be needed for low-speed motors.

The use of multiple-tooth stator poles in switched reluctance motors has been reported to develop more torque than the conventional single-tooth per pole construction [5] and [6], at the expense of a slightly less convenient stator pole structure, especially in motor construction and winding. Multi-tooth machines also have the advantage of requiring less excitation, but suffer from a reduced $\frac{\lambda}{g}$ ratio and therefore a reduced performance. In practice, however, the single-tooth per pole construction has been the most commonly used.

2.1.3 Number of phases

The choice of the phase number is influenced in a major way by the required starting torque from any rotor position. To ensure adequate starting torque at all rotor angles there must be adequate overlapping of poles adjacent to the airgap and in the main magnetic circuit. To provide a reversible drive which develops torque at any rotor position, a motor with at least three phases is required and this could have six stator poles and four rotor poles, although other stator and rotor pole combinations are possible.

In general, introducing more poles and phases produces less torque ripple, but also increases the cost of the machine (the more phases the machine have, the more power semiconductor switches in the inverter). Increasing the number of poles and phases makes the exciting frequency of the stator phases to be higher for the same speed. Also as mentioned in subsection 2.1.2, increasing the number of poles and phases can create some losses . In this thesis, however, only the three-phase 6:4 pole configuration SRMs are considered as the focus is on high speed, traction applications.

2.2 Inductance variation and static torque production

To produce torque, the switched reluctance motor must be designed such that the stator winding inductances vary with the position of the rotor. The inductance is a maximum when a rotor pole is aligned with the stator pole of the excited phase (see Fig. 2.3) and is at a minimum when the rotor pole and the stator pole are completely misaligned (see Fig. 2.4). It should be noted that the torque is independent of the direction of current flow, so that unidirectional currents can be used, permitting a simplification of the electronic driving circuits. The electronic circuits will be dealt with in Chapter 3.

In general, because of magnetic nonlinearities, the torque T must be calculated in terms of change of energy W or co-energy W' as

$$T(\theta, i) = \frac{\partial W'(\theta, i)}{\partial \theta}, \tag{2.2}$$

where θ is the angle describing the rotor position and i is the phase current. The co-energy is the area given by

$$W' = \int_0^i \psi di. \tag{2.3}$$

Changes in co-energy depend both on the angular position of the rotor and on the instantaneous

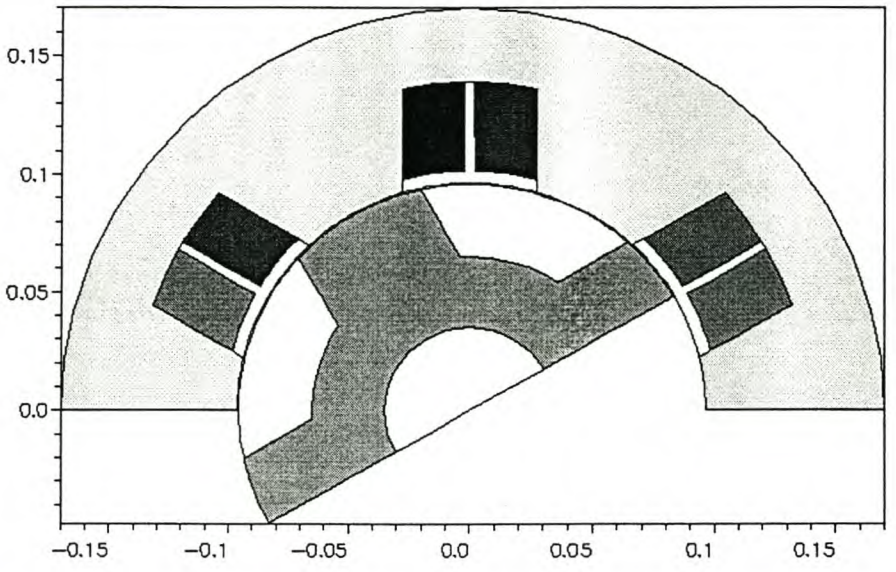

Figure 2.3: **The rotor aligned with the excited stator pole**

values of the current. If magnetic saturation is neglected then the torque equation could be simplified to

$$T(\theta, i) = \frac{i^2}{2}\frac{\partial L}{\partial \theta} Nm, \tag{2.4}$$

where L is the self inductance of the circuit at any value of θ. From this equation it can be seen that the torque does not depend on the direction of the current but on the inductance variation with the rotor position. The number of cycles of inductance variation per revolution is proportional to the number of rotor pole pairs, and the length of this cycle is equal to the rotor pole pitch. Fig. 2.5 illustrates clearly the inductance variation and torque production. The figure is divided into regions, to show different stages of inductance variation and torque production.

R01: at θ_0 the 'leading' edges of rotor poles meet the edges of stator poles and the inductance starts an ideally linear increase with rotation, continuing until the poles are fully overlapped at θ_1, when the the inductance reaches its maximum value Lmax.

R12: from θ_1 to θ_2 the inductance remains constant at Lmax, through the region of complete overlap.

R23: from θ_2 to θ_3 the inductance decreases linearly to the minimum value, Lmin.

R34: from θ_3 to θ_4 the stator and the rotor poles are not overlapped and the inductance remains constant at Lmin.

Eqn. 2.4 above can best be explained with the aid of Fig. 2.5(b). It can be seen from this figure that torque is a function of the inductance variation, the torque can be controlled to give

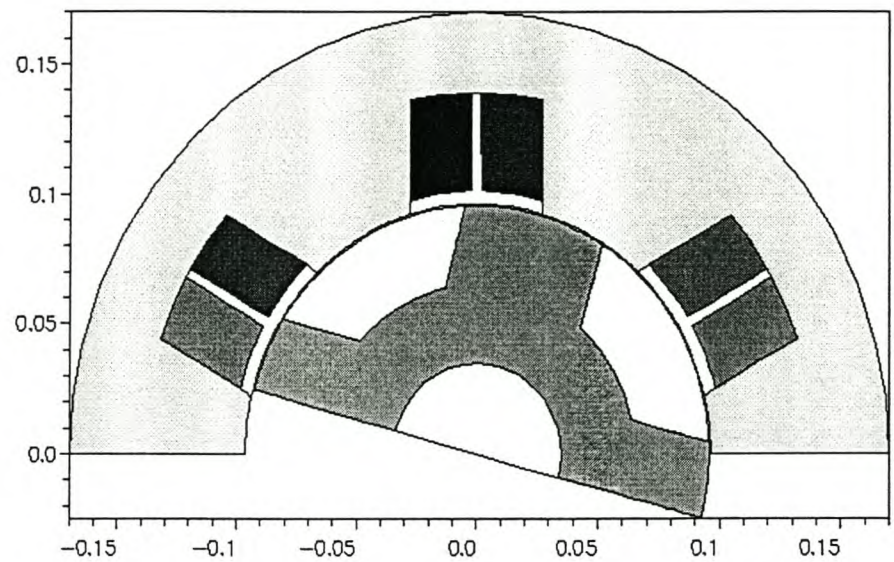

Figure 2.4: **The rotor misaligned with the exited stator pole**

a resultant which is positive (for motor action) or is negative (for generator action) simply by switching the phase current on and off at appropriate instants during the inductance cycle. It can also be noted that between θ_1 and θ_2 the inductance is constant and by eqn. 2.4 the torque in these positions must be zero. Throughout this cycle the phase current should be kept constant. The equation also tells us that with constant current i and ideally constant $\frac{dL}{d\theta}$, the torque will be constant.

2.3 Voltage equation and energy flow

The terminal voltage for one phase is given by:

$$v = Ri + \frac{d\psi}{dt}, \tag{2.5}$$

where v is the voltage applied across the winding and ψ is the flux linkage. If there is no saturation, the slope of the $\psi - i$ curve is the inductance at the particular rotor angle, and this is equal to the ratio of flux linkage to current, therefore

$$\frac{d\psi}{dt} = L\frac{di}{dt} + i\frac{dL}{dt}, \tag{2.6}$$

but at the rotational speed ω, $dt = \frac{d\theta}{\omega}$ and substituting this equation into the second term of the right hand side of eqn. 2.6 we get,

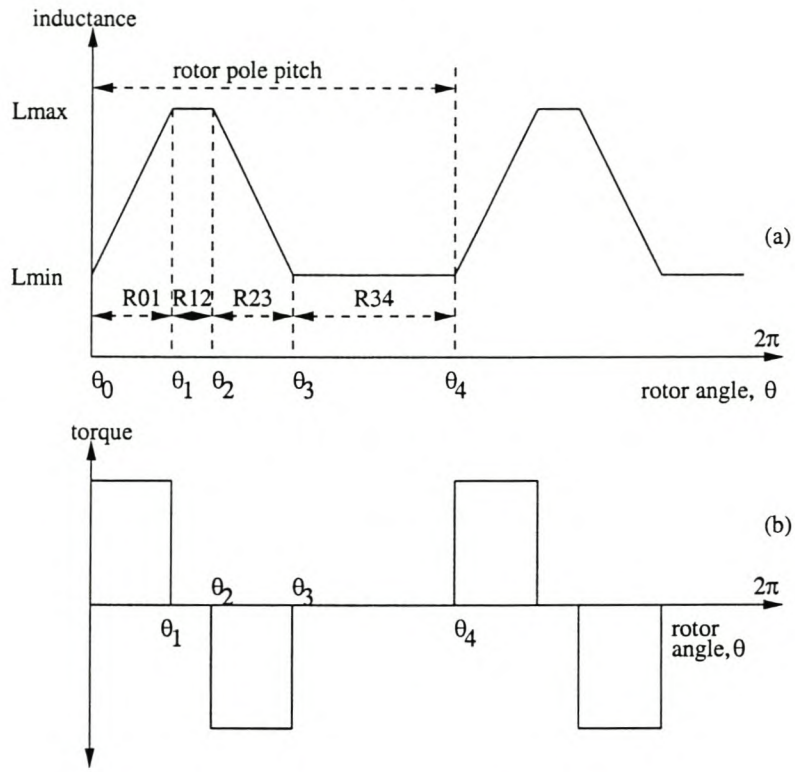

Figure 2.5: **(a) Assumed linearised variation of inductance of a stator inductance as a function of rotor position**
(b) the corresponding variation of torque with constant current.

$$\frac{d\psi}{dt} = L\frac{di}{dt} + i\omega\frac{dL}{d\theta}. \tag{2.7}$$

If we assume there is magnetic linearity and furthermore negligible resistance, then

$$v = L\frac{di}{dt} + i\omega\frac{dL}{d\theta}. \tag{2.8}$$

The inductance term limits the current into the machine and as such needs to be minimised in order to minimise kVA-power that must be handled by the converter. The second term on the right of eqn. 2.8 is the speed voltage given by

$$e = i\omega\frac{dL}{d\theta}. \tag{2.9}$$

If eqn. 2.8 is multiplied with i, the rate of change of energy (input power) is given by

$$vi = iL\frac{di}{dt} + i^2\frac{dL}{d\theta}\omega \tag{2.10}$$

but the stored energy is given by

$$\frac{d}{dt}\left[\frac{1}{2}Li^2\right] = iL\frac{di}{dt} + \frac{i^2}{2}\frac{dL}{d\theta}\omega \tag{2.11}$$

therefore

$$vi = \frac{d}{dt}\left[\frac{1}{2}Li^2\right] + \frac{i^2}{2}\frac{dL}{d\theta}\omega \tag{2.12}$$

This equation shows that the input electrical power goes partly to increase the stored magnetic energy ($\frac{1}{2}Li^2$) and partly to provide mechanical output power, which is

$$P_m = T\omega = \frac{i^2}{2}\frac{dL}{d\theta}\omega. \tag{2.13}$$

According to [7], the stored energy in the magnetic field is not necessarily dissipated. With the appropriate converter circuit it can be recovered to the supply at the end of the period of rising inductance.

2.4 Current and flux waveforms

In the SRMs all current and flux waveforms are nonsinusoidal and those of current vary widely with operating conditions. Fig. 2.6 shows diagrammatically one cycle of the waveforms of current and flux, typical of the motoring condition in which the winding is switched on at some angle θ_i, in advance of the onset of rising inductance region. The effective inductance of the circuit is $Lmin$, initially, so allowing the current to build up rapidly to its maximum value and to maximise its torque producing effect. Subsequently, the rising inductance and the motional e.m.f. cause the current to fall until the switch is opened at some angle θ_x, before the maximum inductance is reached. Thereafter, the current falls more rapidly because an opposing polarity is applied to the winding by virtue of the current flowing into the supply.

The angle between θ_i and θ_x is referred to as the conduction angle θ_c. It is of considerable importance for the control of the machine. If we assume negligible resistance, as long as a positive voltage is applied, the flux increases at a steady rate (see eqn. 2.5 and, when a negative voltage is applied, the flux also decreases at a steady rate). The maximum flux always occurs at the instant of switch-off defined by θ_x.

Analytically, Fig. 2.6 can be explained by the following equations:

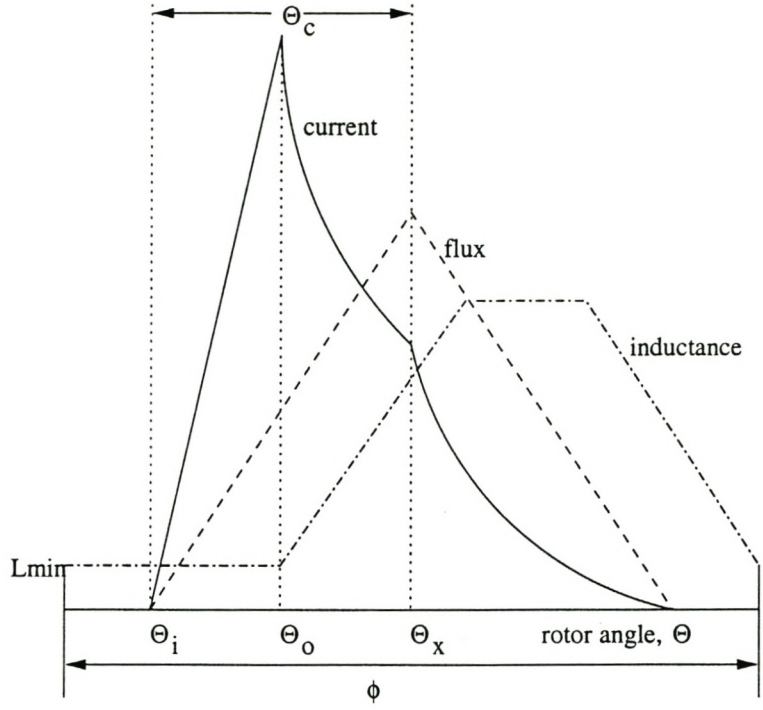

Figure 2.6: **Current and flux waveforms at switch-on and switch-off**

$$\frac{d\psi}{dt} = \frac{d\psi}{d\theta}\frac{d\theta}{dt} = L\frac{di}{d\theta}\frac{d\theta}{dt} + i\omega\frac{dL}{d\theta} \tag{2.14}$$

$$\frac{d\psi}{d\theta}\omega = L\frac{di}{d\theta}\omega + i\omega\frac{dL}{d\theta}, \tag{2.15}$$

therefore

$$\frac{d\psi}{d\theta} = L\frac{di}{d\theta} + i\frac{dL}{d\theta}. \tag{2.16}$$

Chapter 3

Converter Topologies and SRM Drive

This chapter briefly deals with different kinds of converter topologies used for SRM's and look at their different performance and device count. The second part deals with the whole SRM drive system and operation. It deals in particular with current control and the use of position feed-back in commutation.

3.1 Design considerations

SRM's unlike the dc and ac (synchronous or induction) machines, cannot be simply plugged to a dc or an ac source and be expected to run. A switched reluctance motor requires a converter circuit to control the unipolar phase current in its phase windings. There are various converter configurations that can be employed in running the SRM, but to choose a particular configuration depends on the application of the machine.

In this subsection just a few of the well-known inverter topologies will be introduced . The suitability of a particular inverter circuit changes with the motor geometry, making an absolute general choice impossible [9]. This, however, is in contrast to drives operating with sinusoidal voltages or currents where the inverter topology is independent of the motor design. The inverter selection is effectively affected by whether the motor is operating with or without an overlapping current in its speed range and also by the number of stator/rotor poles. The most commonly used inverters are:

- the conventional inverter (two-switch per phase configuration) (Fig. 3.1),
- the bifilar winding inverter (Fig. 3.2),

- the split dc link inverter and
- the C-dump inverter (Fig. 3.3).

In the conventional inverter given in Fig. 3.1 the phases are independent, unlike in the ac inverter where the motor windings are connected between the midpoints of adjacent inverter phase legs. The motor winding is in series with both switches, providing valuable protection against shoot-through faults. Each switch is rated to withstand the dc supply voltage.

The upper and lower phaseleg switches of a phase are switched on together at the start of each conduction period or working stroke. The lower phaseleg switch remains on during the conduction period, while the upper phaseleg switch is 'chopped' by a control strategy such as the current regulator control and voltage-PWM control. At the end of the conduction period both switches are turned off and any remaining stored magnetic energy that is not converted to mechanical work is returned to the supply by the current freewheeling through the diodes. The main disadvantage with this circuit is the total number of switches used.

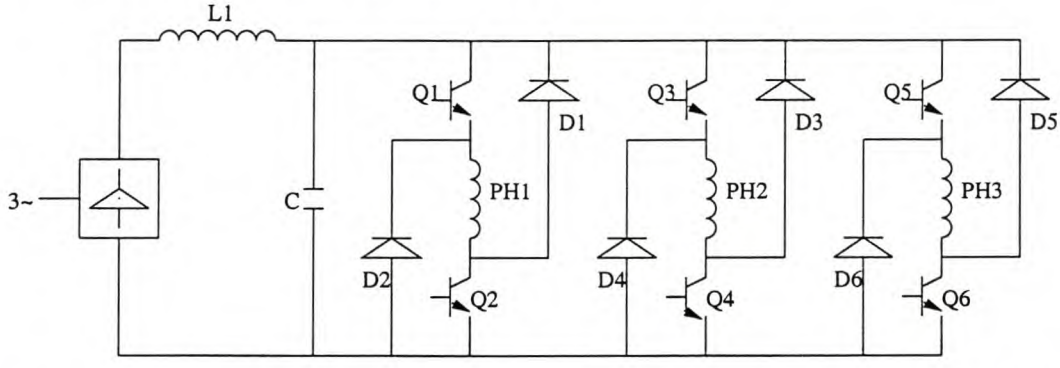

Figure 3.1: **A conventional two-switch per phase inverter for a three-phase SRM**

The bifilar inverter given by Fig. 3.2, unlike the conventional converter, requires only one switch per phase but the switch voltage rating is very high (more than double the dc supply voltage). Also the imperfect coupling between the primary and the secondary phase windings causes voltage spikes to appear across the phase switches during switch-off, this requires snubbing to protect the switches. Copper is poorly utilised as a result of the need to double the number of connections in bifilar inverters. The main advantages are that it requires one switch per phase and that it is useful for applications where the supply voltage is sufficiently low such that switches of $2V_s + \Delta V$ rating are of little penalty [10].

The split power supply inverter is not considered in this thesis because it is more suitable for machines with an even number of phases, and the machine considered in this thesis is a three-phase machine, an odd phase numbered machine.

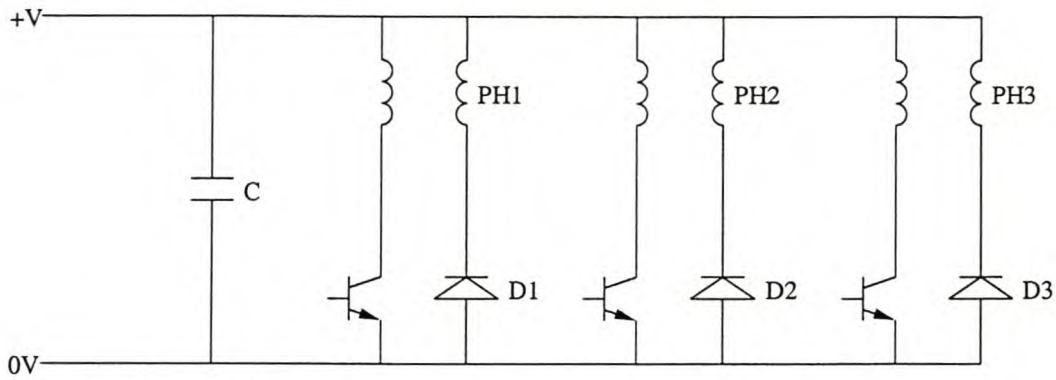

Figure 3.2: **A bifilar inverter for a three-phase SRM**

Another inverter to be considered is the C-dump inverter of Fig. 3.3. The number of switches in the C-dump inverter is reduced to equal the number of motor phases plus an additional switch to bleed the stored energy from the dump capacitor back to the supply via the stepdown chopper. The dump capacitor voltage is maintained at a level above the dc supply voltage and can be controlled in such a way as to optimise the motor phase current waveform. The main disadvantage occurs in the case of control failure in the energy recovery circuit which would result in the rapid build-up of charge on the dump capacitor, so protective measures are needed to avoid failure of the entire converter from overvoltage.

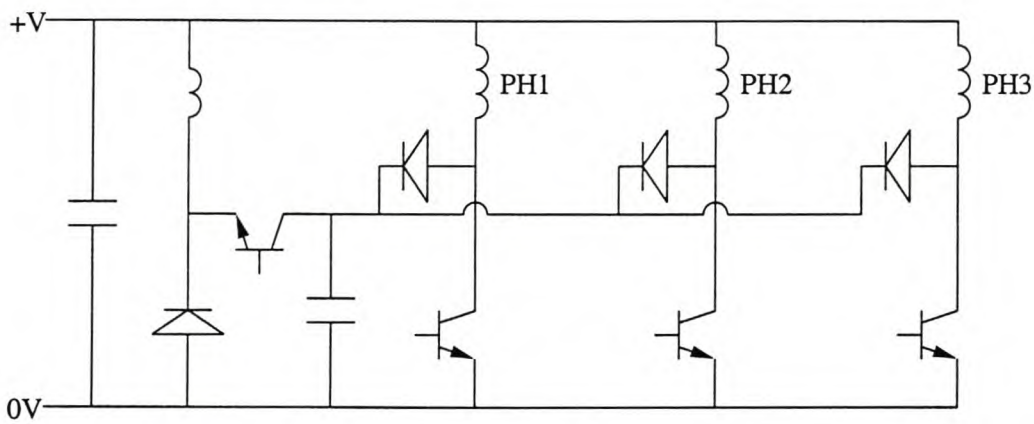

Figure 3.3: **A C-dump inverter for a three-phase SRM**

The actual inverter that is used in this thesis is shown in Fig. 3.4. It can be noted that this inverter is a standard phase-arm inverter in a four quadrant mode. This means that the inverter allows AC current and voltage in the phase windings, independently of each other. The phase windings, as expected from the SRM inverter are connected in series between the active switches. The phase-arms were already available in the laboratory and therefore this inverter was used for testing the SRM. This inverter has the highest number of semiconductor switches of all the inverters discussed above and therefore it is susceptible to more semiconductor losses.

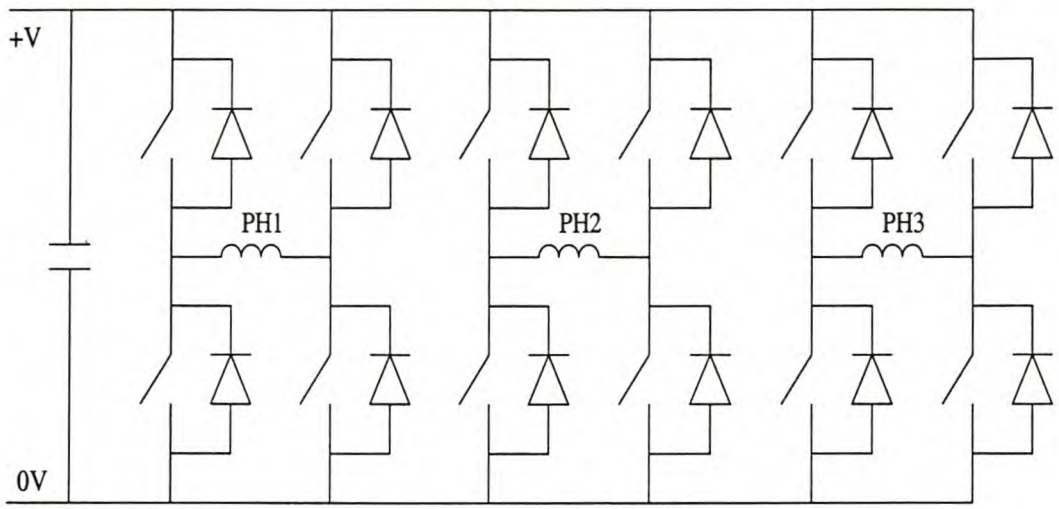

Figure 3.4: **Inverter adapted for SRM**

3.2 Current control and position feedback

For motoring operation the pulses of phase current must coincide with a period of positive rate of change of inductance, i.e. when a pair of rotor poles is approaching alignment with the stator poles of the excited phase. The timing and dwell of the current pulse determine the torque, the efficiency, and other parameters. With fixed firing angles, there is a monotonic relationship between average torque and r.m.s. phase current, but in general it is not very linear. This may present some complications in feedback-controlled systems although it does not prevent the SR motor from achieving 'near-servo-quality' dynamic performance, particularly in respect of speed range, torque/inertia, and reversing capability [11]. The general structure of the simple control scheme is much the same as that of the brushless dc drive.

SRMs have got various methods of control. Just to mention a few, there are (i) the position sensorless control where the incremental inductance is detected and the rotor position is estimated, (ii) the position feedback control where a position sensor is mounted on the shaft of the machine and the rotor position is sensed and fed back into the control system and (iii) the fuzzy logic control.

During excitation of a phase winding the current must be limited by chopping the applied voltage. This can be achieved by using the upper switch to chop the voltage whilst the lower switch remains on throughout the conduction period. Fig. 3.5 illustrates current control by means of a current regulator to maintain approximately constant current in the phase winding, irrespective of the rotor speed. By controlling the reference input, the torque of the motor can be controlled. This form of control requires wide bandwidth current transducers in series with each phase winding.

At high speed, the current is limited by the high induced speed voltage (eqn. 2.9) and the

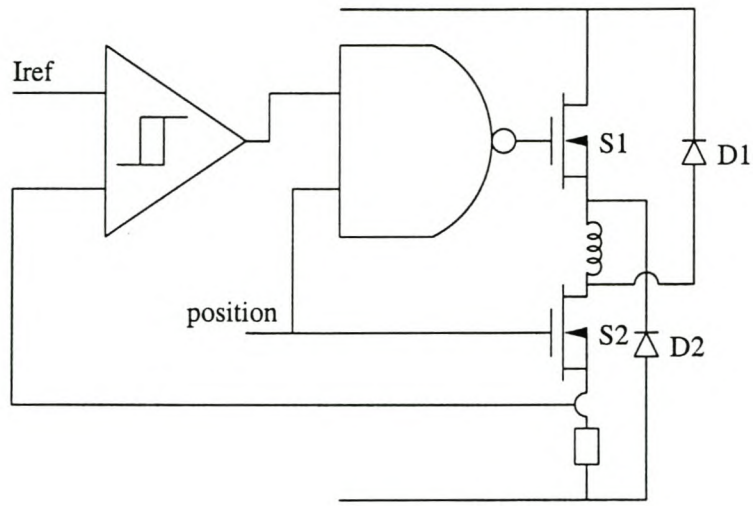

Figure 3.5: **Hysterisis current control of a SRM-phase winding**

switching frequency of the power device is relatively low. Current waveforms of that shown in Fig. 2.6 are then obtained. A four pole rotor running at 1500 rpm will require a switching frequency of only 100 Hz in this mode of operation. At low speeds the phase current is chopped and controlled by a comparator with hysteresis for setting the minimum and maximum current chopping levels (shown in Fig. 3.5). The switching frequency of the upper power switch using hysterisis current control depends on the reference levels and the resistance and inductance of the phase winding. As the phase inductance changes with rotor position, the switching frequency also changes in this case.

Chapter 4

SRM Design and Optimisation

To design an optimum SRM, analytical methods such as the lumped circuit analysis method does not give accurate results due to the complex nonlinear magnetic circuit of the machine, and can therefore not be employed. The finite element method (FEM) seems to be the best method to use in the optimum design of these machines. This chapter will therefore start by describing the design optimisation criteria and the method used in the SRM design optimisation. It further discusses the FEM and lumped circuit analysis and compares some of their results. The chapter also gives the optimisation results of both the tapered stator pole and the straight stator pole machines.

4.1 Design optimisation

The SRM can have a wide range of stator to rotor pole ratios. In this thesis the 6:4 combination was chosen because for normal speeds the number of rotor poles and the number of phases must be kept as low as possible [8]. The two machines, i.e. the tapered and straight stator pole machines were optimised using the finite element method directly in the optimisation process as will be described in Section 4.2. Also it is worth mentioning that not only certain variables of the machine were optimised. An attempt was made in this study to optimise all the important dimensions of the machines.

Consequently four variables were selected in the optimisation for both the tapered and straight pole SRMs, as shown in Figs. 4.1 and 4.2, respectively. These are the stator slot width (st_sw), the stator inner diameter (st_id), the stator yoke height (st_yh), and the rotor tooth width (ro_tw). In the case of the straight pole machine, the stator pole width instead of the stator slot width is optimised. The stator outer diameter, the stack length and the airgap length were kept

constant in the optimisation process.

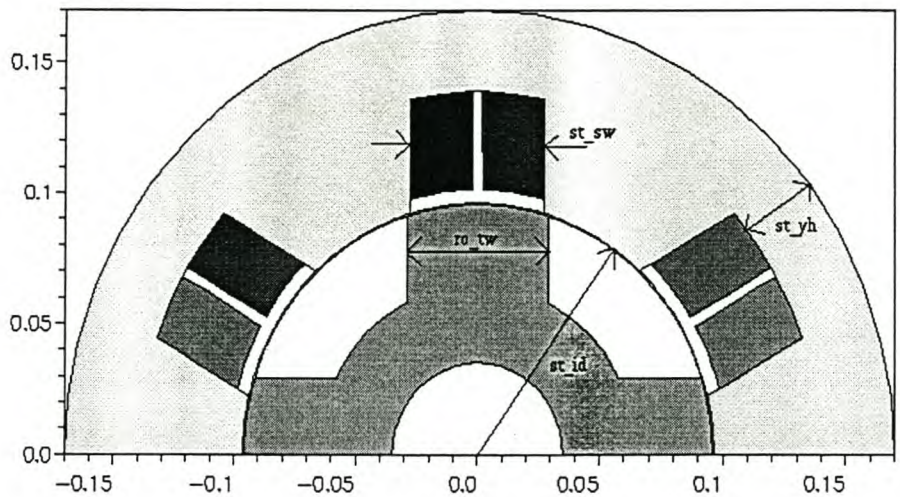

Figure 4.1: **Tapered stator pole machine showing optimised variables**

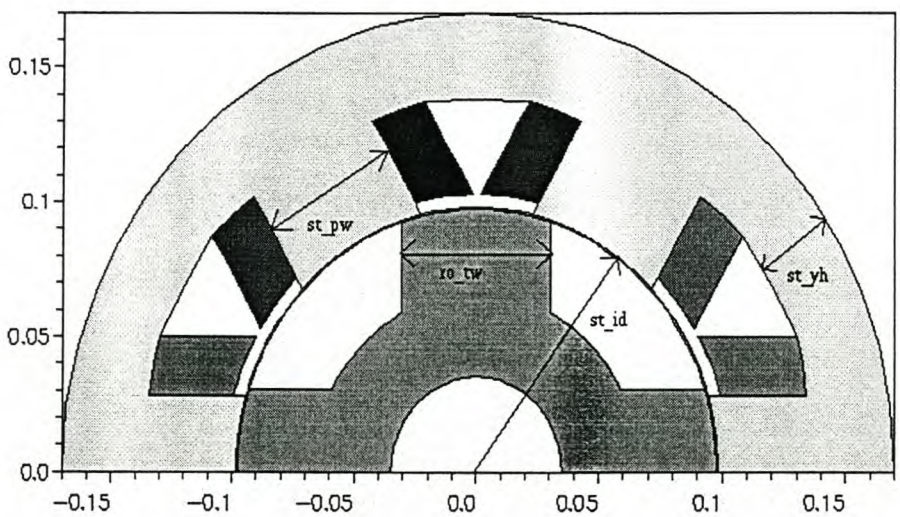

Figure 4.2: **Straight stator pole machine showing optimised variables**

The performance parameter that is maximised in the optimisation process is the average torque of the SRM per rated copper losses. The torque of the SRM is developed by the tendency of the rotor poles to align with the excited pair of stator poles. This developed torque at constant current, however, is not constant but varies with rotor position. It was therefore decided to use the average phase-torque as the performance parameter to be maximised. By maximising the average torque instead of, peak torque, a wider torque versus rotor position profile is obtained and hence a lower torque ripple. The equation for calculating the average torque is given by:

$$T_{ave} = \frac{1}{\tau}\int_0^{\tau} T(\theta)d\theta \tag{4.1}$$

where $\tau = \frac{\pi}{4}$ for a 6:4 machine and $T(\theta)$ is the torque at position θ. In discrete format eqn. 4.1 becomes

$$T_{ave} = \frac{1}{n}\sum_{i=1}^{n} T(i) \tag{4.2}$$

where n is the number of steps the rotor is rotated in the finite element analysis from the unaligned to the aligned position and $T(i)$ is the finite element calculated torque at step i. The real problem with a two-dimensional FEM is that it does not take into account the end-effects like stator end-windings and hence flux linkage due to these end-windings. When the rotor and the stator are unaligned, the airgap between the stator and the rotor becomes very large such that only little flux passes through from the stator to the rotor. The machine will then have some additional losses due to end winding flux leakage.

4.2 FEM Analysis

The finite element method has proved to be particularly flexible, reliable and effective in the analysis and synthesis of power-frequency electromagnetic devices [15]. The finite element software used in the design optimisation of the SRM is not of the commercial variety. It makes use of the triangular elements of the first order. Only one pole (stator and rotor) of the machine is meshed with one airgap macro-element [22] comprising nodals on both sides of the airgap. A time-saving scheme has been devised by [21] and [20] that makes the use of one airgap element very attractive to time-step the rotor in the FE analysis. The Newton-Raphson method is used for the solution of non-linear equations [20].

The finite element solution has the following basic steps:

- Mesh generation
  The accuracy of the finite element solution is dependent on the mesh topology. The mesh is thus an important part of any finite element model and a lot of attention should be placed on creating it [15].
  In the FEM package used in this study the mesh is generated by defining all the nodes in the machine (see Appendix A). The accuracy of the solution will then depend on the number of nodes defined and their location, i.e. some regions in the motor require more nodes than

other regions depending on the flux distribution.

Only one stator slot of the machine is outlined in terms of xy-coordinates and meshed and mirrored to the number of slots over a pole pitch. The phase windings are then allocated to the slots. Also, one half of a pole of the rotor is outlined and meshed and mirrored to the other half pole. The stator and rotor meshes are then joined. The meshed structures of both the tapered and straight stator pole SRMs are shown in Figs. 4.3 and 4.4.

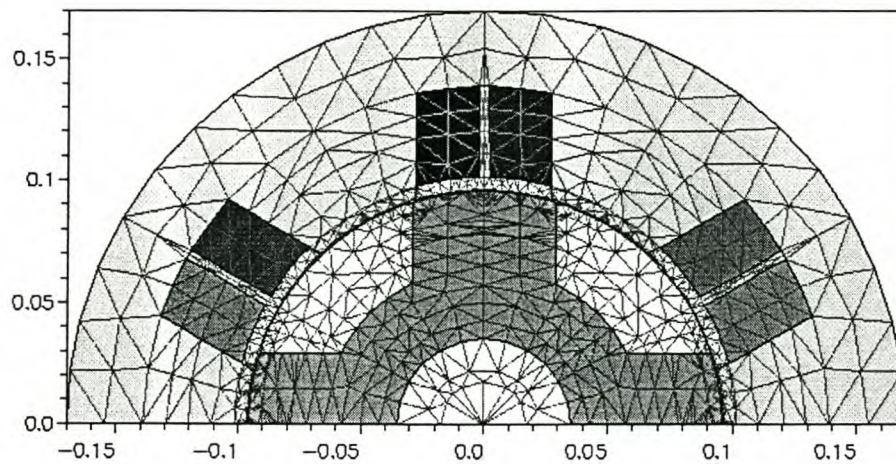

Figure 4.3: **Meshed diagram of a tapered stator pole SRM**

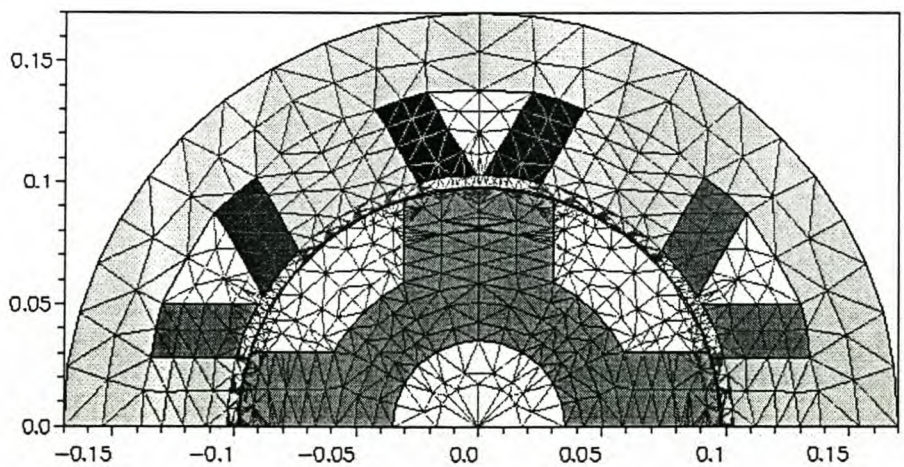

Figure 4.4: **Meshed diagram of a straight stator pole SRM**

- Pre-processing

  The pre-processor is where the finite element model is created. This step is necessary to save storage and calculation time. Sparse matrices are created and the numbering of equations is optimised to minimise the solution time.

- Solving
  The solver (see Appendix B) creates a finite element mesh and solves it. The Newton-Raphson solution procedure is used to solve for magnetic vector potential at different nodes. It is a solution of a set of non-linear equations due to the non-linearity of the magnetic materials.

- Post-processing
  The post-processor calculates field quantities such as the flux linkages, inductances, etc. from the known nodal magnetic vector potentials.

The finite element program determines the equivalent circuit parameters and use them to calculate the output parameters. To calculate the equivalent circuit parameters, the winding resistance R_{phase} is calculated from the active copper area at a temperature of 100^0C as well as the length of the machine and the number of conductors. The copper area is determined from the given slot dimensions. To calculate the flux linkages λ using the finite element method it is necessary to specify the phase currents I_{phase} of the machine. The phase current and the phase resistance can then be used to calculate the copper losses P_{cu}, given by

$$P_{cu} = I_{phase}^2 R_{phase} \tag{4.3}$$

or

$$P_{cu} = qI_{rms}^2 R_{phase} \tag{4.4}$$

where q is the number of phases, thus $I_{rms} = \frac{I_{phase}}{\sqrt{q}}$ and

$$I_{phase} = \sqrt{\frac{P_{cu}}{R_{phase}}}. \tag{4.5}$$

For a three phase machine the conduction angle $= 30^0$.

The finite element field solutions are used directly in the optimisation procedure to optimise the machine in multi-dimensions as illustrated by Fig. 1.1. The algorithm of Powell is used for the optimisation. Powell's method is an unconstrained optimisation algorithm that minimises a function without calculating derivatives [17]. The method minimises (maximises) with each iteration r of the optimisation process, the function value or performance parameter of the machine along a set of n vector directions, where n is the number of variables to be optimised. The initial set of n vector directions is the unit or co-ordinate directions. After each iteration, a new direction is defined which is used in the set of vector directions for the next iteration and a new mesh is

generated according to the changed set of vector directions. The complete explanation of this procedure is given in [18].

The optimisation software procedure was developed by [18] and was used likewise. When the finite element program is called by the optimisation procedure the rotor is rotated in the finite element program through an angle of 45^0 in steps of 3^0, i.e. from non-alignment to alignment. According to Fig. 1.1, during this optimisation process the performance parameter [Y] is calculated and the optimisation procedure uses eqn. 4.2 to calculate this parameter . The phase current is allowed to vary during this process for both the tapered stator pole and the straight stator pole machines. The phase current depends on the phase resistance as shown by eqn. 4.3 and 4.5. The copper loss is kept fixed throughout this process. The flux plots from the finite element solution of both machines at both the aligned and unaligned positions are given by Figs. 4.5 - 4.8.

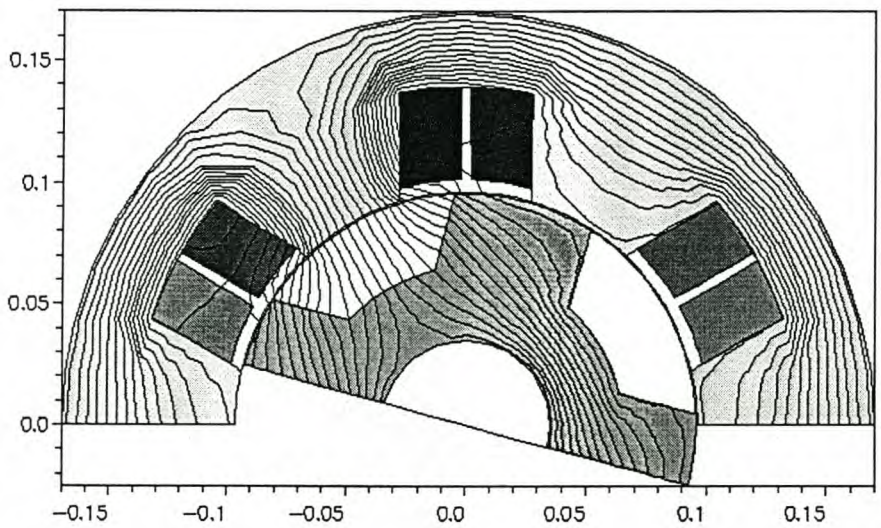

Figure 4.5: **Flux plot of the finite element solution of the tapered stator pole SRM - unaligned position**

4.3 Lumped circuit analysis

To verify some FEM calculated results it is necessary to consider the lumped circuit model (LCM) diagram of the machine. The lumped circuit diagram of the switched reluctance motor for one phase is given in Fig 4.9, where $\Re_1$ is the effective stator reluctance, $\Re_2$ is the effective rotor reluctance, $\Re_g$ is the airgap reluctance, Ni is the applied mmf and ϕ is the flux. This lumped circuit diagram was implemented by considering regions of the magnetic circuit (see Fig. 4.10) which have a specific flux density. Three regions were identified, namely, the stator core, the air

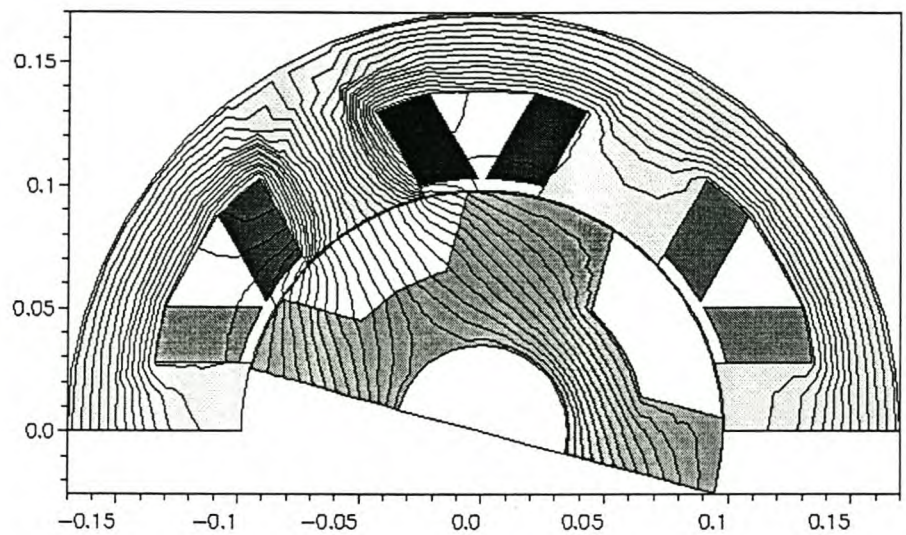

Figure 4.6: **Flux plot of the finite element solution of the straight stator pole SRM - unaligned position**

gap and the rotor core. A typical B-H magnetization curve of the electric machine steel was used in the calculation of the phase inductances to take saturation into account.

The following procedure was used:

Firstly, the following symbols must be defined as they are going to be used in the equation to follow. A_g, A_1, A_2 are the cross-sectional areas of the air-gap, stator core and rotor core, respectively, g, l_1, l_2 are the lengths of the air gap, stator core length and the rotor core length, respectively, and $\mu_0$and $\mu_r$are the permeability of the air and the relative permeability of the iron core, respectively.

First, a ϕ was selected and used in the following equations to calculate the flux densities and hence the relative permeabilities

$$A_g = \frac{A_1 + A_2}{2}, \tag{4.6}$$

$$B_1 = \frac{\phi}{A_1}, \tag{4.7}$$

and determine H_1 from the B-H curve;

$$B_2 = \frac{\phi}{A_2}, \tag{4.8}$$

and determine H_2 from the B-H curve. Then calculate the relative permeabilities as follows:

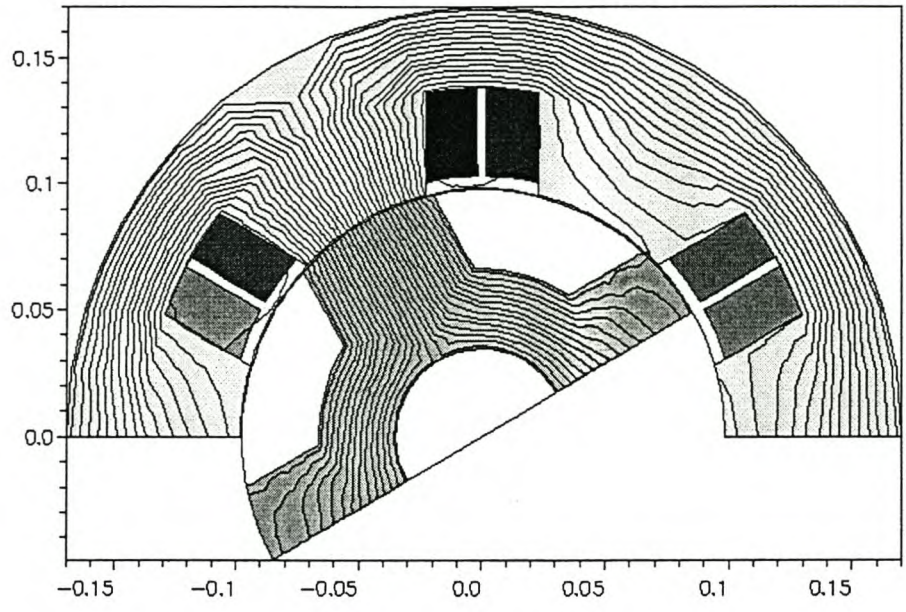

Figure 4.7: **Flux plot of the finite element solution of the tapered stator pole SRM - aligned position**

$$\mu_{r1} = \frac{B_1}{\mu_0 H_1}, \tag{4.9}$$

$$\mu_{r2} = \frac{B_2}{\mu_0 H_2}, \tag{4.10}$$

where $B_1$and B_2 are the stator and rotor magnetic flux densities, respectively.

The relative core permeabilities are in turn substituted in the following equation to calculate a new flux value, $\phi\prime$

$$Ni = \phi\prime\Re \tag{4.11}$$

$$\phi\prime = \frac{Ni}{\Re} \tag{4.12}$$

where $\Re = 2\Re_g + \Re_1 + \Re_2$ and

$$\Re_g = \frac{g}{\mu_0 A_g}, \tag{4.13}$$

$$\Re_1 = \frac{l_1}{\mu_0 \mu_{r1} A_1}, \tag{4.14}$$

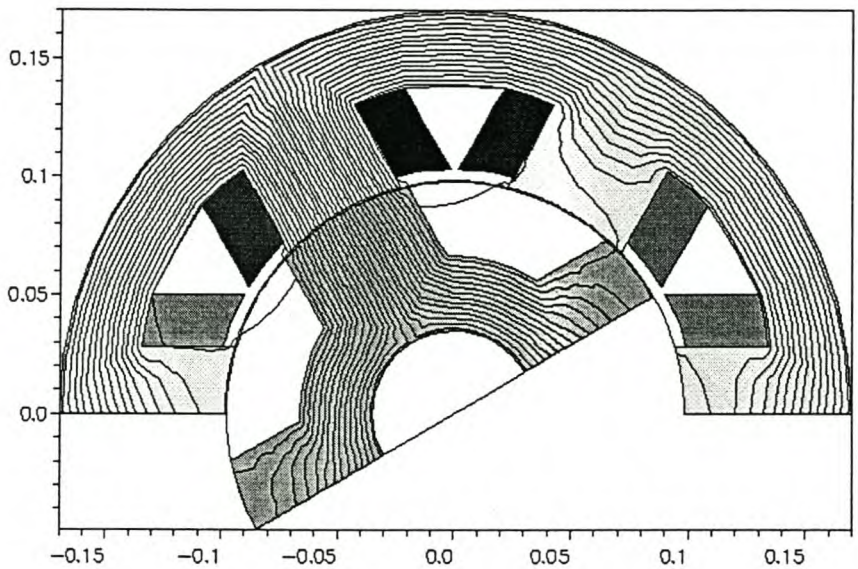

Figure 4.8: **Flux plot of the finite element solution of the straight stator pole SRM - aligned position**

$$\Re_2 = \frac{l_2}{\mu_0 \mu_{r2} A_2}, \tag{4.15}$$

and

$$\phi\prime = \frac{Ni}{\left[\frac{2g}{\mu_0 A_g} + \frac{l_1}{\mu_0 \mu_{r1} A_1} + \frac{l_2}{\mu_0 \mu_{r2} A_2}\right]} \tag{4.16}$$

The new $\phi\prime$ is then compared with the selected value of flux ϕ and if they are not equivalent, a new value is selected using the bisection method. If they are equivalent the calculation is taken further to calculate the phase inductance using

$$L = \frac{N_{phase}\phi}{i}. \tag{4.17}$$

Inductances were calculated and compared using the FEM analysis and lumped circuit (LCM) analysis at two current levels, viz. 50 A and 219 A at the aligned position. The values are given in Table.4.1. It can be observed from Table.4.1 that the values obtained using the two different methods correlate and, thus, confirms the FEM results. It must be mentioned that this comparison was done at the aligned position only as the procedure to calculate the LCM values for the unaligned position is more complex and not that accurate, because of the large air gap.

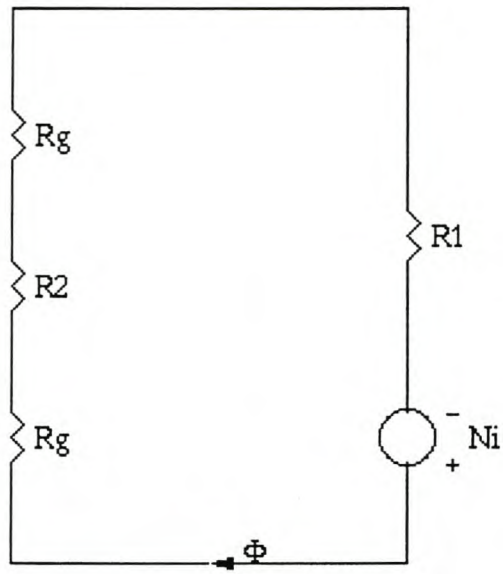

Figure 4.9: **Per phase magnetic lumped circuit of the SRM**

Table 4.1: **FEM and LCM results of flux linkages and inductances**

I (A)	λ (FEM)(Wb.t)	L (FEM)(mH)	λ (LCM)(Wb.t)	L (LCM)(mH)
50	1.502	30.046	1.736	34.720
219	1.946	8.886	2.058	9.397

4.4 Some optimisation results

The optimum dimensions obtained from the optimisation of both machines are given in Table 4.2. The optimised structures are shown in Figs.4.11 and 4.12.

The geometric ratios of the machines are calculated from the results of the optimised structures and are given in Table 4.3. The optimum geometric ratios published in literature [12],[13],[14] are also given in Table 4.3. These ratios have been optimised for straight pole SRMs with fixed MMFs rather than fixed copper losses, as in this paper. Apart from FEM, other numerical methods have also been used by other authors for SRM optimisation, see [12],[13].

Note that in Table 4.3:

$t_s = st\_pw$ (stator pole width),

$t_r = ro\_tw$ (rotor tooth width) and

$\lambda_s$and λ_r are the stator and rotor pole pitches respectively.

It is clear from Table 4.3 that some of the optimum ratios of the two SRMs compares favourably with each other and also shows good correlation with the ratios given by literature. The main

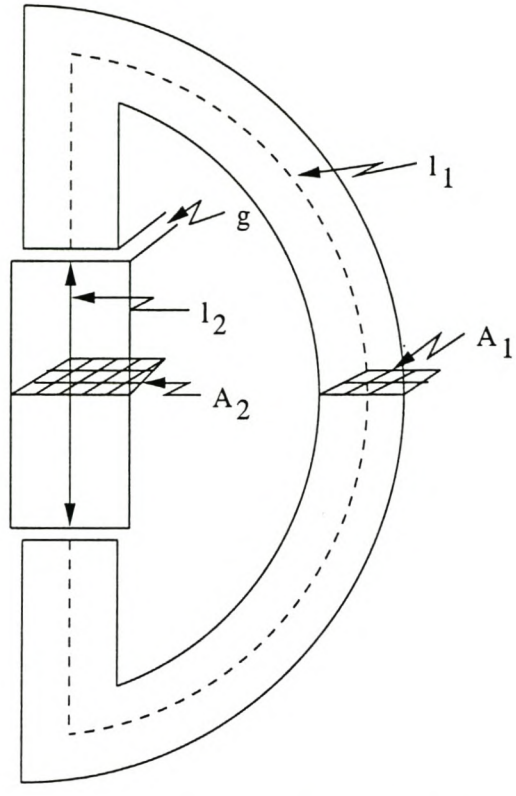

Figure 4.10: **Aligned magnetic circuit of the SRM (the two stator yokes are put and used together as one yoke).**

differences in the ratios of the tapered and straight pole SRMs occur in the $\frac{t_s}{\lambda_s}$ and $\frac{t_s}{t_r}$ ratios. These are also evident from the machine structures shown in Figs. 4.11 and 4.12. It can be observed that there are also differences in the $\frac{t_s}{\lambda_s}$ and $\frac{t_r}{\lambda_r}$ ratios of the straight pole SRM and that given by the literature.

Table 4.2: **Dimensions of SRMs (the symbol '*' implies the dimensions that were varied in the optimisation).**

Dimensions (mm)	Tapered	Straight
st_od	340.0	340.0
st_id *	192.63	196.51
st_sh	42.67	39.88
st_pw *	-	45.78
st_sw *	54.96	-
st_yh *	31.02	31.87
ro_od	191.39	195.27
ro_shd	70.0	70.0
ro_yh	30.0	31.41
ro_tw *	60.0	62.82
sp_tip	26.85^0	23.55^0
sp_base	37.19^0	33.05^0
stack length	175	175
g	0.62	0.62

Table 4.3: **Geometric ratios**

	Tapered	Straight	Literature (straight)
$\frac{t_s}{\lambda_s}$	0.447	0.55	0.4-0.5
$\frac{t_s}{g}$	162.68	165.95	>150
sr	0.563	0.574	0.57-0.63
$\frac{t_r}{\lambda_r}$	0.399	0.4096	<0.5
$\frac{t_s}{t_r}$	0.752	0.902	-
bc	1.14	1.12	-

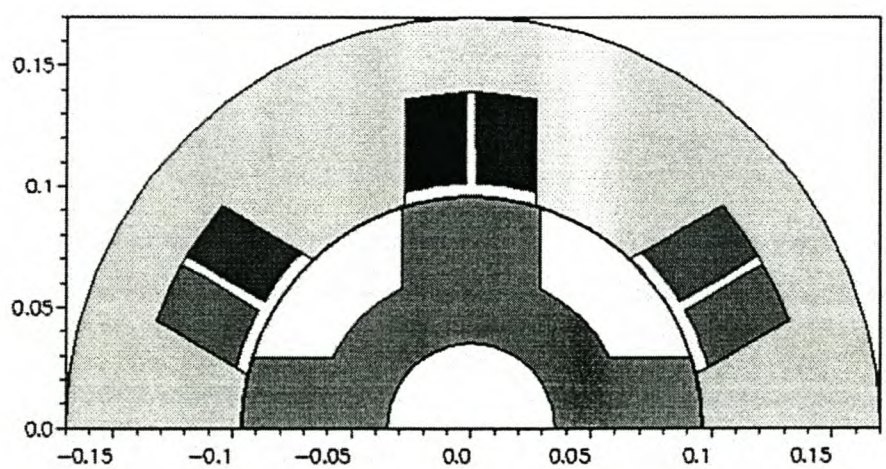

Figure 4.11: **Optimised structure of the tapered pole SRM (Power rating is above 50 kW)**

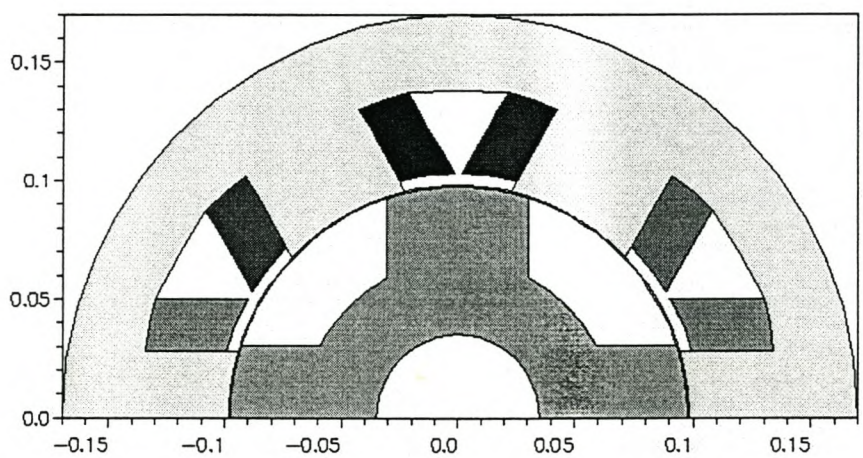

Figure 4.12: **Optimised structure of the straight pole SRM (Power rating is 50 kW)**

Chapter 5

Tapered and Straight Pole Design Comparison

This section describes the torque-angle characteristics of the optimised tapered and straight pole SRMs with the phase currents fixed and the rated copper losses the same. It must be mentioned that the results presented in this section are FEM calculated results only.

5.1 FEM calculated results and comparison

Figs. 5.1 and 5.2 show the torque angle profiles of both machines with only one phase active. The irregularities in the peak torque of the straight pole SRM (see Figs. 5.2 and 5.1) are due to the inadequate meshing of the stator and rotor poles. The actual torque curve is very smooth. The torque-angle profiles of the two machines are compared in Fig. 5.3. Hence, it is clear that the tapered pole machine produces a higher peak torque (9%) compared to the straight pole machine, with the plateau widths of the torque curves very much the same. Furthermore, it can be seen from these figures as suggested by [3], that tapering leads to a fuller torque-angle characteristic near the aligned position. The torque-slope towards alignment (45^0) of the tapered SRM shown in Fig. 5.1 is steeper than that of the straight pole SRM shown in Fig. 5.2.

Fig. 5.4 shows the torque versus rotor position of the tapered and straight pole SRMs with two phases active according to their switching angles (0^0 to $45^0$and 30^0 to 75^0, respectively). This figure shows the amount of torque ripple produced by the tapered and straight pole machines. It is clear that the torque ripples are very much the same , with the torque ripple of the tapered machine showing a slight improvement in the average torque. The straight stator pole machine also shows a torque pulse which is not good while the tapered stator pole machine has a smoother

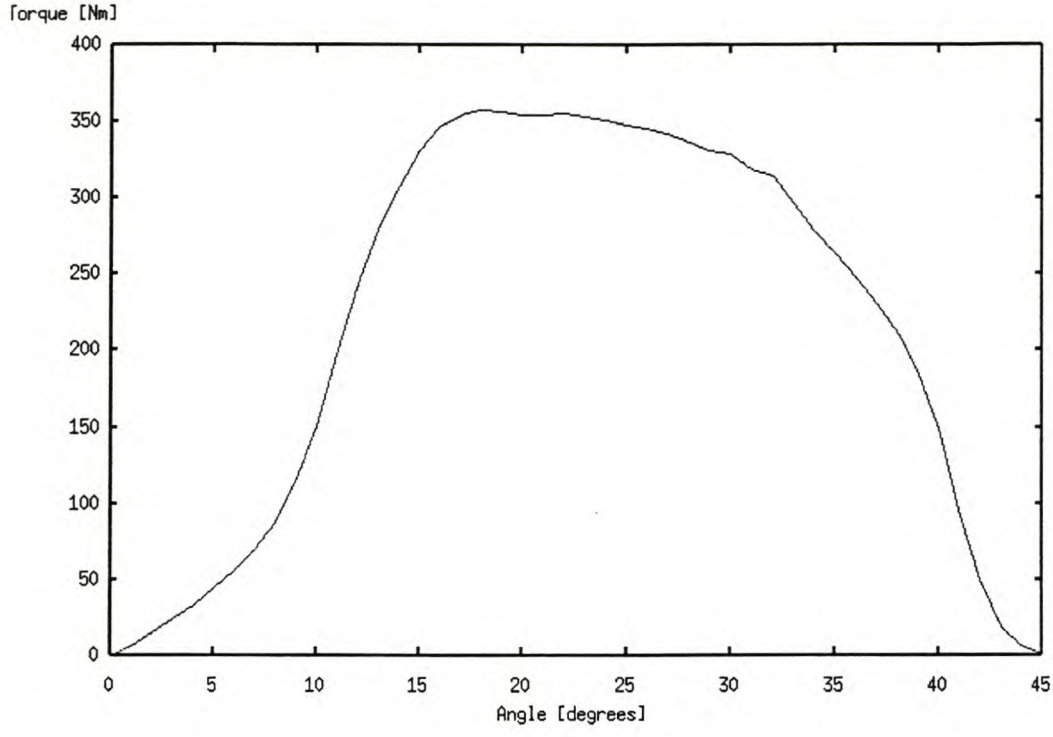

Figure 5.1: **Phase-torque versus rotor position of the tapered pole SRM with the copper losses fixed at 1.5 kW**

variation. Table 5.1 summarises the improvement in average and peak torque of the tapered pole machine in comparison with the straight pole machine for one phase active.

Table 5.1: **Peak and average phase-torque of the tapered and straight pole SRMs at rated copper losses**

Torque (Nm)	Tapered	Straight	Improvement
T_{ave}	196.5	182.5	7%
T_{peak}	332	302	9%

Typical variations of flux-linkage with phase current are shown in Fig. 5.5 for both the tapered and the straight pole machines. Here the rotor is fixed at two positions, the aligned and the unaligned positions whilst the current is allowed to vary form zero to rated current. It can be observed that saturation is maximum at the aligned position and that there is no evidence of magnetic saturation in the unaligned position, this should be expected because of the very large airgap that results from this position. It can also be observed that for low current levels, the curves are quite linear for both the aligned and the unaligned positions.

The converted energy, W (electrical energy converted to mechanical energy) per stroke could be computed from a knowledge of the area enclosed between the aligned and unaligned curves. The average electromagnetic torque T is then given by

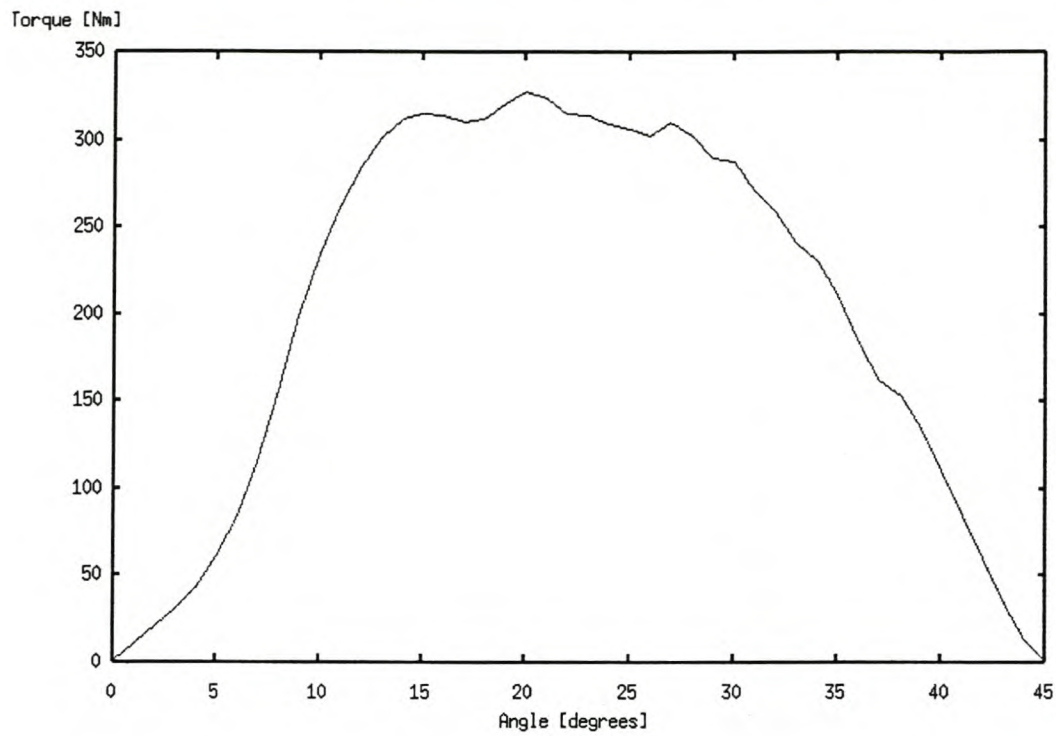

Figure 5.2: **Phase-torque versus rotor position of the straight pole SRM with the copper losses fixed at 1.5 kW**

$$T_{ave} = qN_r \frac{W}{2\pi} \tag{5.1}$$

where qN_r, the number of steps per revolution, is given by the product of the phase number q and the rotor pole number N_r. It becomes clear from eqn. 5.1 that in order to get the most torque per ampere of phase current, the converted area W must be large. Eqn. 5.1 together with Fig. 5.5 can then be used to explain the improvement of the peak torque in the tapered stator pole machine compared to the straight stator pole machine. The difference between the areas (areas enclosed by the aligned and unaligned curves) of the tapered and straight stator pole SRMs in Fig. 5.5 has been estimated to be approximately $\approx 10\%$, with the tapered stator pole machine having the larger area. This difference together with eqn. 5.1 justifies the results given in Table 5.1.

Saturation has two important effects on the SRM performance. On the one hand, it limits flux densities for a given current level and thus limits the amount of torque available from the SRM. On the positive side, it tends to lower the required inverter power rating for a given SRM output power and makes the inverter smaller and less costly [19].

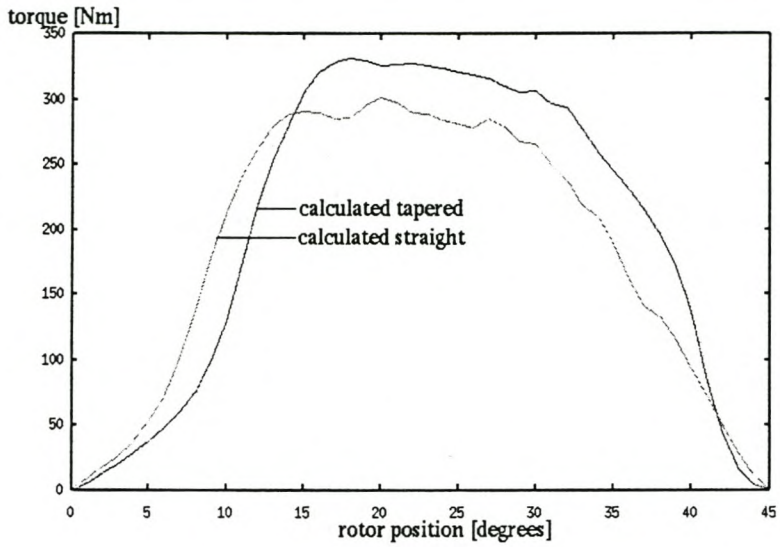

Figure 5.3: **Phase-torque versus rotor position of the tapered and straight pole SRMs for the same copper losses**

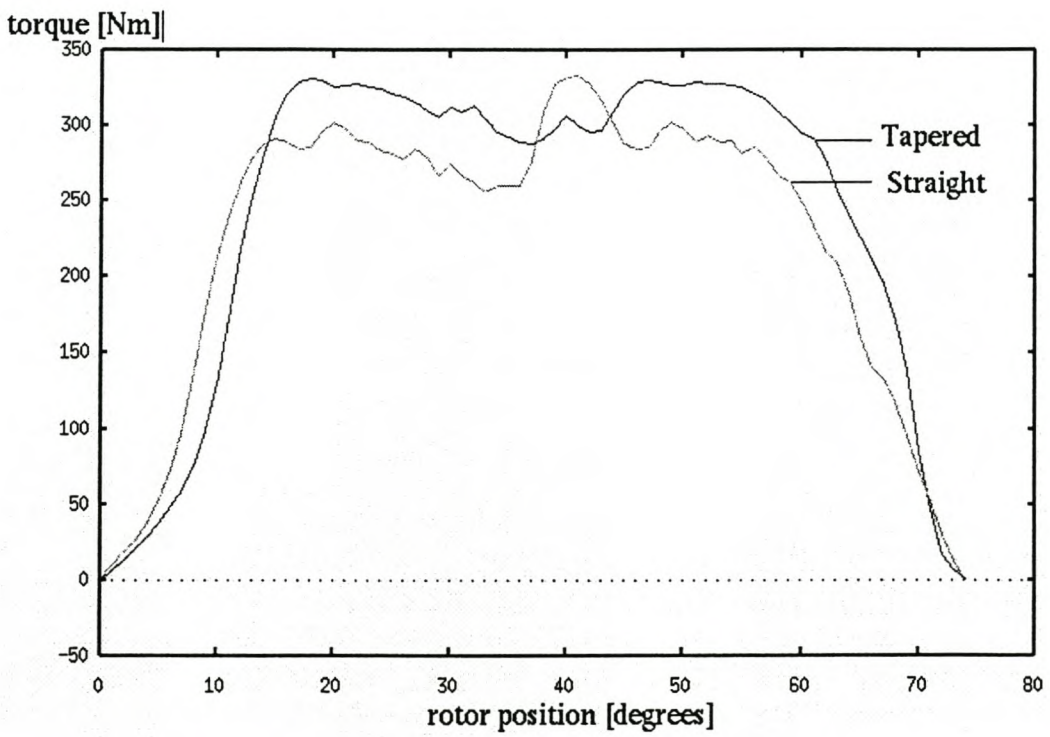

Figure 5.4: **Resultant-torque versus rotor position with two phases active of the tapered and straight pole SRMs (phase A active between $0-45^0$, phase B from $30-75^0$)**

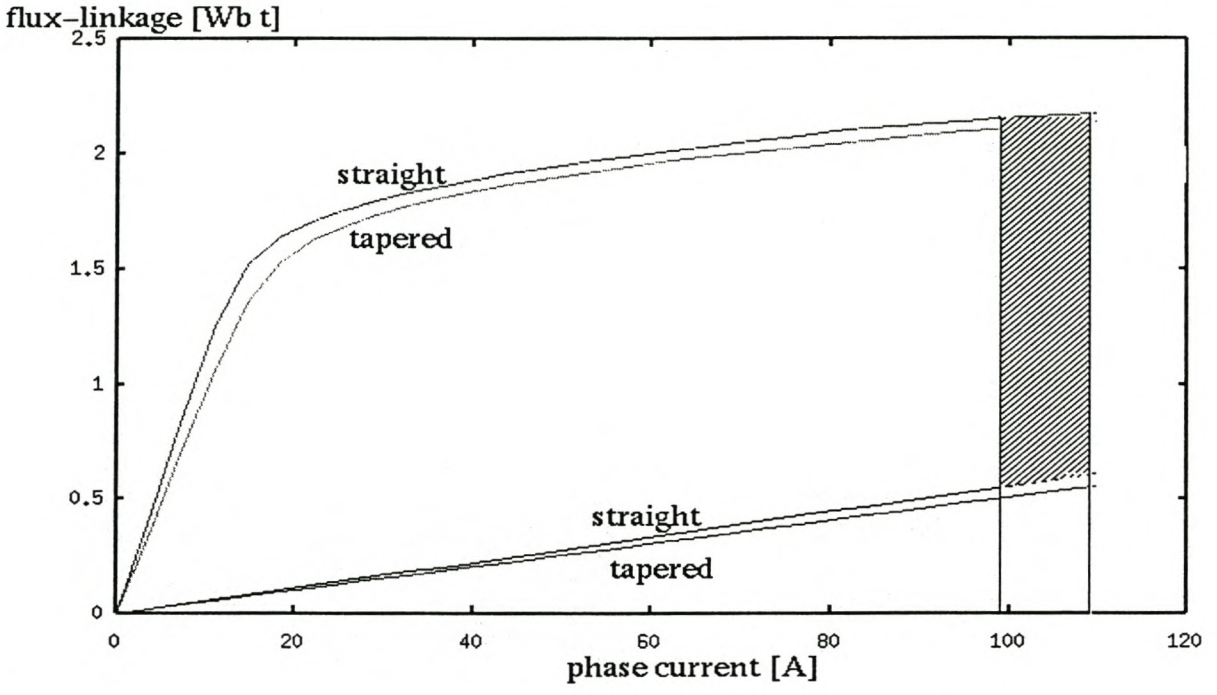

Figure 5.5: **Flux-current characteristics of the tapered and straight stator pole machine in the aligned and unaligned positions (for the same copper losses:** $I_{phase}(straight) = 99A$; $I_{phase}(tapered) = 108.5A$)

Chapter 6

Tests and Results for the Tapered SRM

This chapter deals with testing of the prototype machine. Only the tapered pole prototype machine has been built for testing as it was the interest of this study. This chapter starts by describing the construction of the machine. The SRM drive used is described in terms of the inverter and transputer system used, also the test system which comprises of the loadcell and the associated bracket to measure static torque is discussed. Lastly the static measured and FEM calculated results are compared.

6.1 Machine construction

The tapered SRM is made up of thin sheets of laser cut laminations that are compressed together to form the stator and the rotor (see Fig. C.1 in Appendix C), to eliminate or minimise the eddy current losses. The rotor and the stator laminations are made of the same type of steel (26 ga M19 C5).

The SRM consists of 6 stator poles and 4 rotor poles which are separated by the air-gap g. The stator is mounted on a metal frame, the rotor shaft is also mounted on the frame with bearings on both sides of the shaft to allow the rotor to rotate. The stator yoke is separated from the outer frame by a thin layer of aluminium (the layer of aluminium will act as the airgap between the stator core and the frame) to eliminate flux pulsations in the frame that will otherwise lead to additional core losses. The yoke serves as a return path for the pole flux.

The stator poles are tapered and the machine windings (see Fig. C.2 in Appendix C) are found only on the stator. The winding coil is embedded in stator slots and fitted around a stator pole which is then connected in series with the coil of the diametrically opposite pole to form a phase winding. The winding is secured in the slot by means of a wedge. The winding is made out of

round copper conductors connected in parallel. The diameter of the conductor was calculated from the following formula:

$$d_{cond} = \sqrt{\frac{4 * A_{cond}}{\pi * 0.93^2}}. \tag{6.1}$$

d_{cond} for the machine is calculated as 3.56 mm, but this conductor diameter is too big so other possibilities are looked into such as 4*1.78 mm in parallel or 3*2.00 mm in parallel.

The area of the conductor is $A_{cond} = \frac{2*A_{coil}*fillfactor}{N_{phase}}$. Also see Table 6.1.

Table 6.1: **Optimised performance data**

	Tapered	**Straight**
A_{coil} (mm)	968.39	822.11
A_{cond} (mm)	8.65	7.34
I_{phase} (A)	108.5	99.60
J_{phase} $(\frac{A}{mm^2})$	12.55	13.57
I_{rms} (A)	62.41	57.50
J_{rms} $(\frac{A}{mm^2})$	7.22	7.83
R_{phase} (Ω)	0.13	0.15
P_{cu} (kW)	1.5	1.5
T_{ave} (Nm)	196.5	182.6
L_a $(mH)*$	19.5	19.91
L_u $(mH)*$	5.02	5.57
N_{phase}	112	112

* L_a is the aligned inductance and L_u is the unaligned inductance at the phase current given in the Table 6.1.

6.2 SRM Drive and Test System

For the test of the tapered stator pole SRM the drive system of Fig. 6.1 was used. The motor is controlled by a T800 transputer control system and an analog current regulator together with an IGBT inverter. The position feedback is the input to the transputer control system and all the phase currents are inputs to the analog current regulator. A small resolver is used for the position feedback. With the highest supply that one can get from the laboratory at $380V_{ac}$ one easily obtain $540V_{dc}$ which is more than sufficient.

The inverter that was used is the unipolar three phase inverter and is shown in Fig. 6.2. S1 - S4 in Fig. 6.2 are the IGBT switches per phase. The inverter was initially used for a reluctance

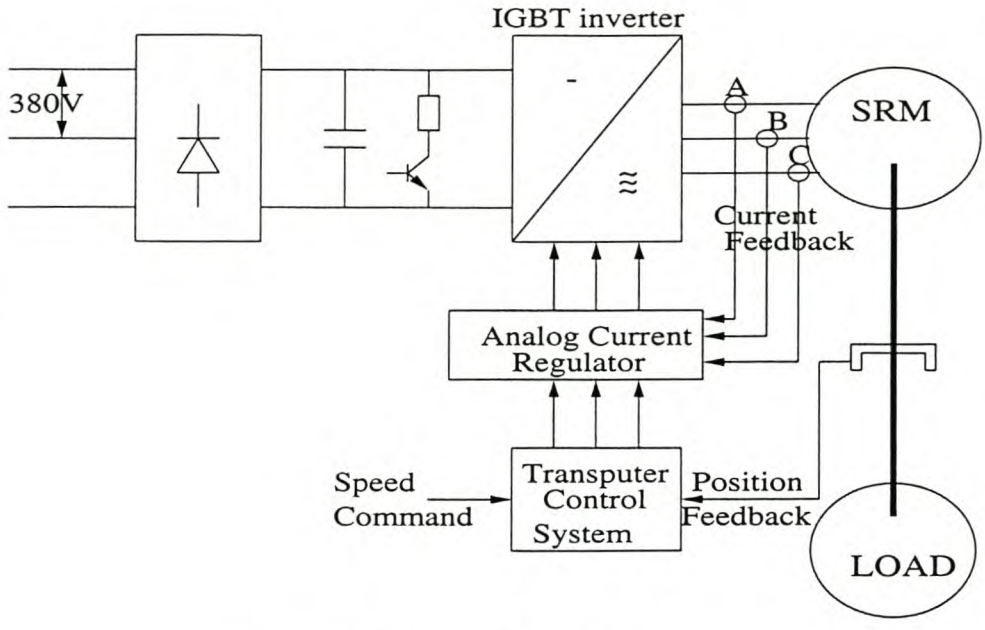

Figure 6.1: **The SRM drive system**

synchronous motor in the laboratory and was adapted to service our purpose as shown, i.e. the windings are connected in series with the active switches.

This figure is for one phase only and it shows how the current is controlled and regulated to switch the IGBT's. The current regulator helps to maintain approximately constant current in the phase winding. The 4.0 kHz into the multiplier represents the switching-frequency of the triangular wave form that is compared with the current error signals for determining switching signals for the switches. This requires wide bandwidth current transducers in series with each phase winding. At low speeds the current is controlled by chopping the applied voltage. It should be noted that the inverter part is capable of four-quadrant operation, with unipolar voltage switching (8.0 kHz effective switching frequency).

For this thesis only the static torque measurements are conducted and the results are discussed and compared in Section 6.3 with the finite element calculations. To measure the static torque of the SRM, a test system comprising of the loadcell and the bracket is used (see Fig. D.1 in Appendix D). The static torque measurements were taken to verify the torque profile of the FEM calculted results. Also there was not enough time to evaluate the running performance of the drive.

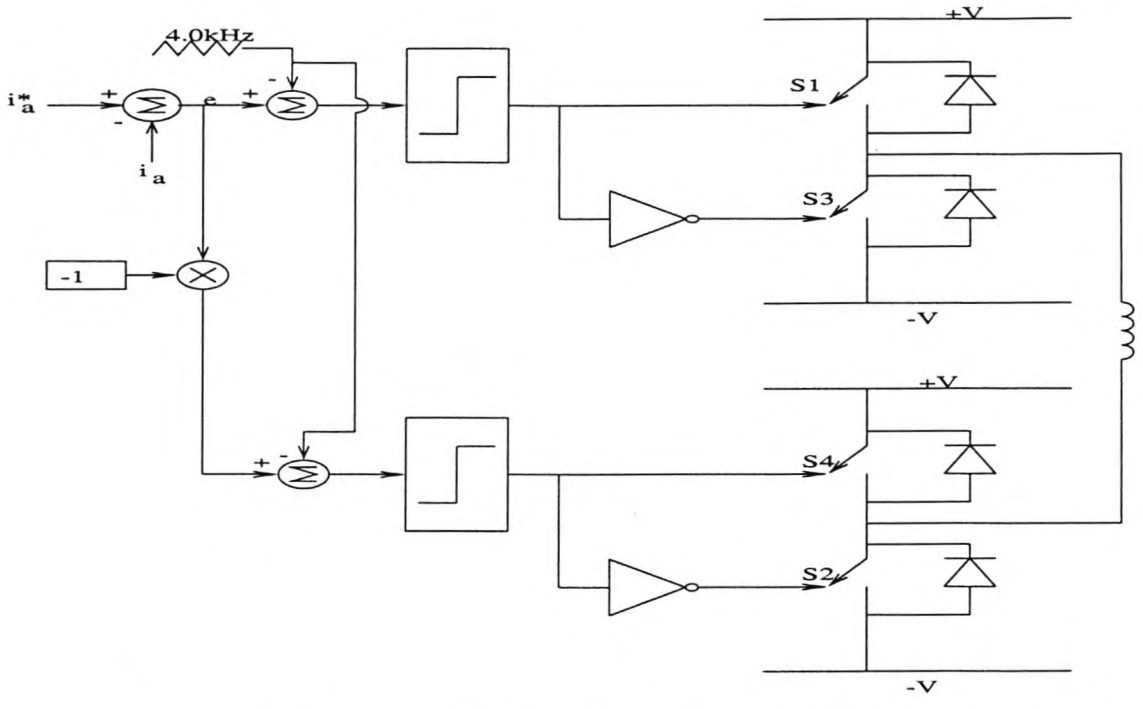

Figure 6.2: **Current control and inverter switches of one phase**

6.3 Comparison of the FEM and measured results

This section focuses on the discussion and comparison of the FEM and measured results of the tapered stator pole SRM. Fig. 6.3 shows the FEM and measured torque-angle characteristics for phase A. Phase A was chosen for no particular reason other than to illustrate the results and to compare the two sets of results. It can be observed from Fig. 6.3 that the two results gives very much the same torque profile. Fig. 6.4 shows the measured torque-angle characteristics for the three different phases. The phases exhibit similarity in terms of the torque profiles. The small differences can be attributed to, amongst other things, the imperfection and the inaccuracy of the available measuring equipment.

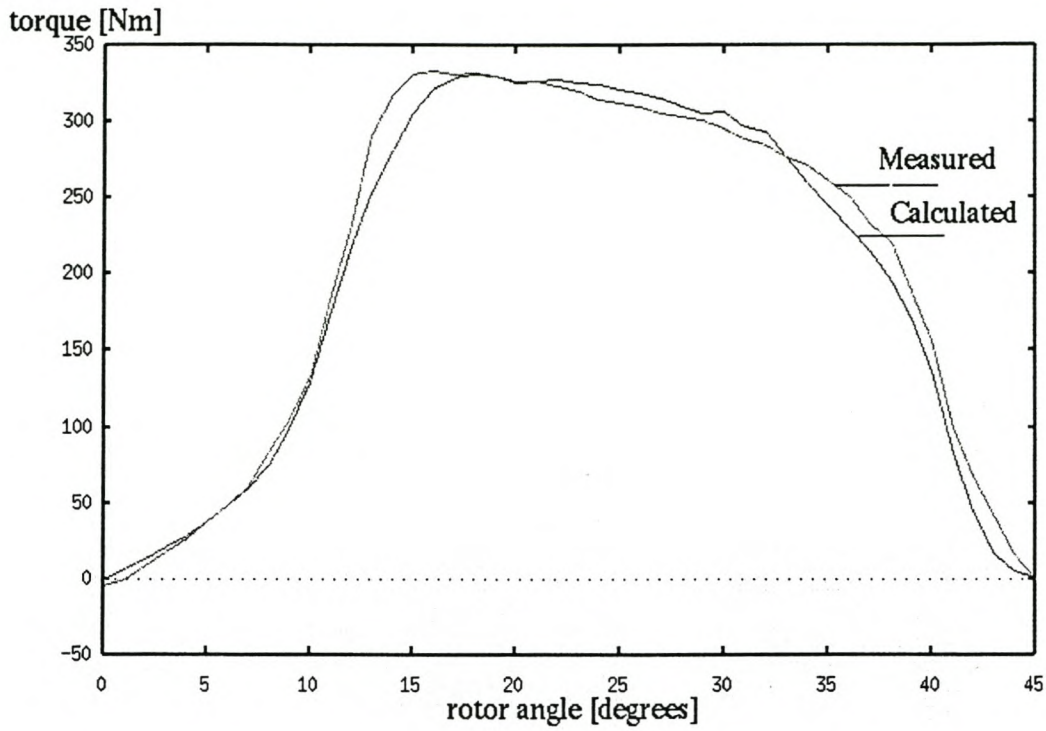

Figure 6.3: Calculated and measured results of torque versus rotor position of the tapered stator pole machine.

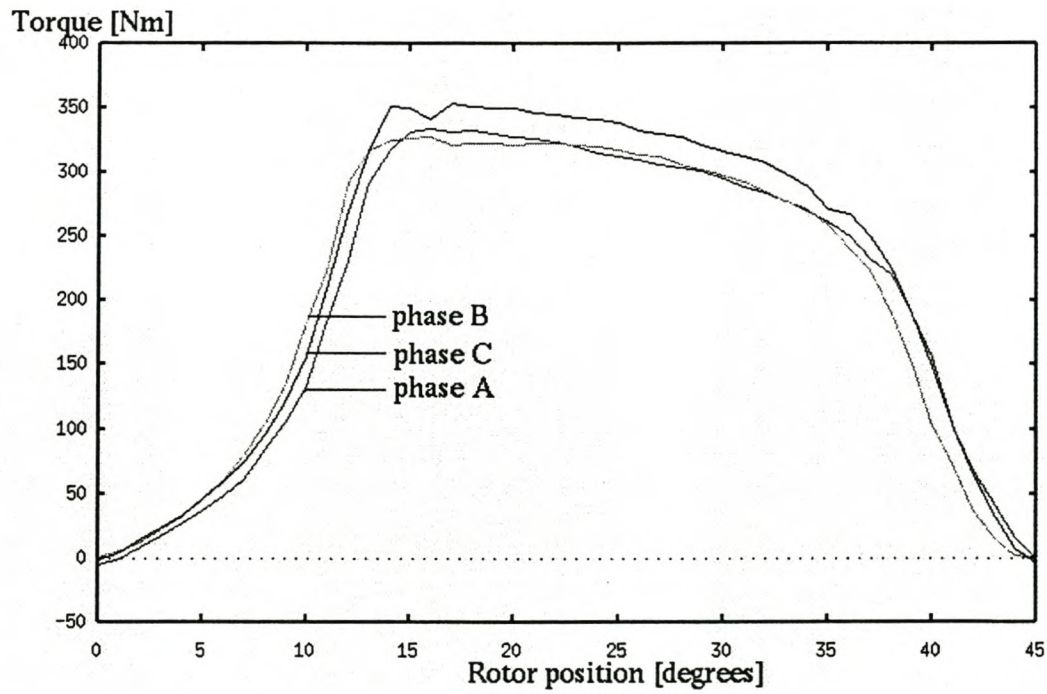

Figure 6.4: Measured results of torque for the three phases

Chapter 7

Conclusions and Recommendations

7.1 Summary of the thesis

The contribution of the thesis can be summarised as the application of the finite element method directly in the design optimisation method for the switched reluctance machine, the construction of the SRM model and evaluation of the static performance characteristics of the machine.

The finite element method is applied directly in the optimisation algorithm to optimise the design of the machine in multidimensions. Due to the nonlinearity of SRMs the FEM offers the best optimum designed machines. It must be mentioned that it is very difficult to design an optimum SR machine using analytical methods. The lumped circuit method is also employed for the purpose of verifying some finite element optimisation results.

Two types of machines are designed and optimised, i.e. the tapered stator pole machine and the straight stator pole machine. Their performance capabilities are evaluated and compared fairly, i.e. same number of turns, same copper losses and same stator outer diameter. The prototype machine has been built and tested to verify the finite element calculations

The conclusions and recommendations are summarised in the sectons below.

7.2 Conclusions

The thesis successfully applied the FEM directly in the optimisation procedure to optimise in multi-dimensions the design of the SRM with the tapered and straight stator poles. The optimisation was focused on maximising the average torque per rated copper losses.

The findings of this study can be summarised as follows:

- The optimum geometric ratios of the tapered and the straight stator pole SRM are found to be different. The optimised straight stator pole SRM was found to possess similar geometric ratios with other SRMs discussed in literature with the exception of a few ratios which are not available, the corresponding ratios for the tapered stator pole machine were not available from literature on SRMs.
- The lumped circuit method was used to confirm the finite element calculated inductances in the aligned position with success. The lumped circuit method however, could not be used for the unaligned position because of the complicated calculations involved due to the large non-uniform airgap.
- Although the 2-D FEM software used did not take into account the end-effects of the windings the measured results did not differ by a considerable margin with the FEM calculated results due to the shorter end-windings in the constructed machine.
- It was also shown that the stator pole tapering significantly improves the peak and average torque of the SRM. It is also found that the torque ripple of the SRM with tapered stator poles is very much the same as with straight stator poles.
- The static torque tests that were performed on the constructed SRM showed a good correlation with the FEM calculated results.

7.3 Recommendations

The following recommendations are made:

- Further work needs to be done to investigate the implications of tapering both the stator and the rotor poles as this was not attempted in this study.
- Vibration tests and stress analysis need to be done on both models (the tapered stator and straight stator pole SRMs)
- Running tests must be done to investigate the performance of the machine at steady-state and under full mechanical loading.
- Nothing has been said in this thesis about the difference in core losses between the tapered and straight pole machines. Although it can be explained in a simply way to be the same, as the fluxes and average core areas are more or less the same, this must be studied in more depth.

Appendix A

Program defining the mesh

```
c      TAPERED STATOR POLE MACHINE
c     sub ee_poly.f.nw
c     To generate Polygons for slots in .pol format.
c     Definition of different rotor shapes and one stator shape
c-----------------------------------------------------------------
c  Variable definition to follow
c--------------------------------
c fim            "From Inch to Meter", a double precision function
c pi             the unexplained constant not avaiable in fortran
c iu             file IO unit as a parameter = 1. Input Unit
c ou             file io unit as a paramter = 13. Output unit
c in_file        For the input data file.
c out_file       For the .pol output file.
c sl_type        "sss" for stator
c n_slots        number of stator slots
c
c unique to the fbr rotor:
c ro_od          outer diameter of rotor
c ro_shfd        shaft diameter of rotor
c ro_tw          rotor tooth width
c ro_th          rotor tooth height
```

```
c ro_yh          rotor yoke height
c
c unique to the stator:
c n_st_st        total number of stator slots
c st_od          outer diameter of stator
c st_id          inner diameter of stator
c st_gw          stator slot gap width
c st_bw          stator slot base (of winding) width
c st_waw         stator winding area width
c st_wid         stator slot top (of winding) width
c st_sht         stator slot height of tooth
c st_shs         stator slot height between gap and top winding
c st_shb         stator slot height between top winding and base
c
c unique to the poly-shapes:
c nseg_pol       number of segments in the poly-shape
c nspnts_pol     number of points in every segment
c nstype_pol     material type of every segment in poly-shape
c npnter_pol     a pointer for the poly-shape to keep trac of numbers
c itpnter_pol    itype_pointer for the poly-shape regions
c x_pol          x-coordinate for the poly-points
c y_pol          y-coordinate for the poly-points
c
c Localised variables:
c i              integer counter
c ap1,ap2        angles for arc
c ainc           angle increments for arc nodes
c nap            number of arc points
c aoff_x         arc x-offset
c aoff_y         arc y-offset
c arcrad         arc radius
c arcang         arc angle
```

```
c arc_x         arc x-point
c arc_y         arc y-point
c spitch        slot-pitc in radians

subroutine ee_pol(in_file,tmp_file,ii,a3, st_ft,st_f1,st_f2,st_f3,i_t1,i_t2,i_t3)
c----------------------
c **            MAIN SUB ENDS OVER HERE                **
c ========================================================
c  four-pole salient rotor
c ========================================================
c Start building the rotor-pole mesh:
c ---------------------------------
        nseg_pol=30
c type for polygons

        do i=1,14
          nstype_pol(i)=0
        end do
        do i=15,30
          nstype_pol(i)=250
        end do

        nspnts_pol(1)=6
        nspnts_pol(2)=6
        nspnts_pol(3)=6
        nspnts_pol(4)=6
        nspnts_pol(5)=7
        nspnts_pol(6)=16
        nspnts_pol(7)=17
        nspnts_pol(8)=8
        nspnts_pol(9)=11
        nspnts_pol(10)=8
```

```
        nspnts_pol(11)=11
        nspnts_pol(12)=7
        nspnts_pol(13)=10
        nspnts_pol(14)=17
        nspnts_pol(15)=8
        nspnts_pol(16)=22
        nspnts_pol(17)=26
        nspnts_pol(18)=26
        nspnts_pol(19)=26
        nspnts_pol(20)=26
        nspnts_pol(21)=22
        nspnts_pol(22)=8
        nspnts_pol(23)=9
        nspnts_pol(24)=8
        nspnts_pol(25)=8
        nspnts_pol(26)=9
        nspnts_pol(27)=8
        nspnts_pol(28)=8
        nspnts_pol(29)=8
        nspnts_pol(30)=8
c
c calculate angles for num points on airgap arc i.e. half pole pitch:
        num=56
        ainc=pi/4.0d0/dble(num)
        angl=ainc
        do i=1,num
          arc(i)=pi/4.0d0+angl
          angl=angl+ainc
        end do
c determine the points of the rotor
c -----------------------------------
c points for region 1
```

```
      x_pol(1,1)= 0.0d0
      y_pol(1,1)= 0.0d0

      arcrad= ro_shfd/2.0d0
      arcang= pi/3.0d0
      call dpolrec(arcrad,arcang,arc_x,arc_y)
      x_pol(1,3)= arc_x
      y_pol(1,3)= arc_y
      x_pol(1,2)= (x_pol(1,1)+x_pol(1,3))/2.0d0
      y_pol(1,2)= (y_pol(1,1)+y_pol(1,3))/2.0d0
      x_pol(1,5)= 0.0d0
      y_pol(1,5)= ro_shfd/2.0d0
      x_pol(1,4)= (x_pol(1,5)+x_pol(1,3))/2.0d0
      y_pol(1,4)= ((arcrad)**2.0d0-(x_pol(1,4))**2)**0.5d0
      x_pol(1,6)= 0.0d0
      y_pol(1,6)= (y_pol(1,1)+y_pol(1,5))/2.0d0

c points for region 2

      x_pol(2,1)= 0.0d0
      y_pol(2,1)= 0.0d0
      arcrad= ro_shfd/2.0d0
      arcang= pi/4.0d0
      call dpolrec(arcrad,arcang,arc_x,arc_y)
      x_pol(2,3)= arc_x
      y_pol(2,3)= arc_y
      x_pol(2,2)= (x_pol(2,1)+x_pol(2,3))/2.0d0
      y_pol(2,2)= (y_pol(2,1)+y_pol(2,3))/2.0d0
      x_pol(2,5)= x_pol(1,3)
      y_pol(2,5)= y_pol(1,3)
      x_pol(2,4)= (x_pol(2,3)+x_pol(2,5))/2.0d0
```

```
          y_pol(2,4)= ((arcrad)**2.0d0-(x_pol(2,4))**2)**0.5d0
          x_pol(2,6)= x_pol(1,2)
          y_pol(2,6)= y_pol(1,2)

c points for region 3

          arcrad= ro_shfd/2.0d0
          arcang= pi/6.0d0
          call dpolrec(arcrad,arcang,arc_x,arc_y)
          x_pol(3,3)= arc_x
          y_pol(3,3)= arc_y
          x_pol(3,1)= 0.0d0
          y_pol(3,1)= 0.0d0
          x_pol(3,2)= 0.5d0*(x_pol(3,1)+x_pol(3,3))
          y_pol(3,2)= 0.5d0*(y_pol(3,1)+y_pol(3,3))
          x_pol(3,6)= x_pol(2,2)
          y_pol(3,6)= y_pol(2,2)
          x_pol(3,5)= x_pol(2,3)
          y_pol(3,5)= y_pol(2,3)
          y_pol(3,4)= (y_pol(3,3)+y_pol(3,5))/2.0d0
          x_pol(3,4)= ((arcrad)**2.0d0-(y_pol(3,4))**2)**0.5d0

c points for region 4-30 are not shown here
c regions have been defined and this program turns half a pole into a full pole
c
        do i=1,nseg_pol
        k=nseg_pol+i
        nspnts_pol(k)=nspnts_pol(i)
        nstype_pol(k)=nstype_pol(i)
                do j=1,nspnts_pol(i)
                l=nspnts_pol(i)+1-j
                x_pol(k,l)=-1.0d0*x_pol(i,j)
```

```
                y_pol(k,l)=       y_pol(i,j)
                end do
        end do
        nseg_pol=nseg_pol*2
c end do nseg reflected

        return
        end
c end of sub rotor_fbr
c
c ========================================================
c tapered stator slot shape
c ========================================================

        subroutine stator_slot_ss(sl_type,spitch, nseg_pol,nspnts_pol,nstype_pol,x_pol,y_pol,
     +  n_st_st,st_od,st_id,st_gw,st_bw,st_wid,st_waw, st_sht,st_shs,st_shb,st_wbw,st_yh,st_wag,st
     +  st_ft,st_f1,st_f2,st_f3,i_t1,i_t2,i_t3)

c----------------------
        pi=2.0d0*dasin(1.0d0)
        spitch=2.0d0*pi/dble(n_st_st)
        itd=0
c
c Start building the stator-slot mesh:
c
        nseg_pol=24
c
c the number of points per segment, and types:
c sections 1 to 12 does the slot whilest sections 13 to 24 covers the lamination around the slot
c
c Region 1: slot-gap opening at bottom-left
        nspnts_pol(1)=13
```

```
        nstype_pol(1)=0
c Region 2: slot-gap opening at bottom-right
        nspnts_pol(2)=13
        nstype_pol(2)=0
c Region 3: slot-gap opening at bottom-far left
        nspnts_pol(3)=12
        nstype_pol(3)=0
c Region 4: slot-gap opening at bottom-far right
        nspnts_pol(4)=12
        nstype_pol(4)=0
c Region 5: top of Section 1 and 3
        nspnts_pol(5)=11
        nstype_pol(5)=i_t1
c Region 6: top of section 2 and 4
        nspnts_pol(6)=11
        nstype_pol(6)=i_t2
c R 7: right of region 5
        nspnts_pol(7)=6
        nstype_pol(7)=0
c R 8: left of region 6
        nspnts_pol(8)=6
        nstype_pol(8)=0
c R 9: top of region 5
        nspnts_pol(9)=8
        nstype_pol(9)=i_t1
c R10: top of region 6
        nspnts_pol(10)=8
        nstype_pol(10)=i_t2
c R11: top of region 7
        nspnts_pol(11)=6
        nstype_pol(11)=0
c R12: top of region 8
```

```
        nspnts_pol(12)=6
        nstype_pol(12)=0
c R13: left of slot-gap opening
        nspnts_pol(13)=18
        nstype_pol(13)=201
c R14: right of slot-gap opening
        nspnts_pol(14)=18
        nstype_pol(14)=201
c R15: far left of slot-gap opening
        nspnts_pol(15)=18
        nstype_pol(15)=201
c R16: far right of slot-gap opening
        nspnts_pol(16)=18
        nstype_pol(16)=201
c R17: top of region 13 and 15
        nspnts_pol(17)=10
        nstype_pol(17)=201
c R18: top of region 14 and 16
        nspnts_pol(18)=10
        nstype_pol(18)=201
c R19: top of region 17
        nspnts_pol(19)=8
        nstype_pol(19)=201
c R20: top of region 18
        nspnts_pol(20)=8
        nstype_pol(20)=201
c R21: top left-middle
        nspnts_pol(21)=9
        nstype_pol(21)=201
c R22: top right-middle
        nspnts_pol(22)=9
        nstype_pol(22)=201
```

```
c R23: far top left
        nspnts_pol(23)=8
        nstype_pol(23)=201
c R24: far top right
        nspnts_pol(24)=8
        nstype_pol(24)=201

c ------------ to start defining areas --------
c
c points for region 1:

        aoff_x=0.0d0
        aoff_y=0.0d0
        arcrad=st_id/2.0d0

        x_pol(1,1)=-st_wid/4.0d0
        y_pol(1,1)=((arcrad)**2.0d0-(x_pol(1,1))**2.0d0)**0.5d0
        x_pol(1,5)= 0.0d0
        y_pol(1,5)= arcrad
        call drecpol( x_pol(1,1),y_pol(1,1),rr,ap1)
        call drecpol( x_pol(1,5),y_pol(1,5),rr,ap2)
        ainc=(ap1-ap2)/4.0

        do i=1,5
        call dpolrec(arcrad,(ap1-ainc*dble(i-1)),arc_x,arc_y)
        x_pol(1,i)=arc_x+aoff_x
        y_pol(1,i)=arc_y+aoff_y
        end do

        arcrad= st_id/2.0d0+st_sht
        x_pol(1,13)=-st_wid/4.0d0
        y_pol(1,13)=((arcrad)**2.0d0-(x_pol(1,13))**2.0d0)**0.5d0
```

```
        x_pol(1,6)= 0.0d0
        y_pol(1,6)= st_id/2.0d0+st_sht

        call drecpol( x_pol(1,13),y_pol(1,13),rr,ap1)
        call drecpol( x_pol(1,6),y_pol(1,6),rr,ap2)
        ainc=(ap1-ap2)/7.0d0
        do i=13,6,-1
        call dpolrec(arcrad,ap1-ainc*dble(13-i),arc_x,arc_y)
        x_pol(1,i)=arc_x+aoff_x
        y_pol(1,i)=arc_y+aoff_y
        end do

c points for region 2:

        aoff_x=0.0d0
        aoff_y=0.0d0
        arcrad=st_id/2.0d0
        x_pol(2,5)= st_wid/4.0d0
        y_pol(2,5)= ((arcrad)**2.0d0-(x_pol(2,5))**2.0d0)**0.5d0
        x_pol(2,1)= 0.0d0
        y_pol(2,1)= arcrad
        call drecpol( x_pol(2,5),y_pol(2,5),rr,ap2)
        call drecpol( x_pol(2,1),y_pol(2,1),rr,ap1)
        ainc=(ap1-ap2)/4.0

        do i=1,5
        call dpolrec(arcrad,(ap1-ainc*dble(i-1)),arc_x,arc_y)
        x_pol(2,i)=arc_x+aoff_x
        y_pol(2,i)=arc_y+aoff_y
        end do

        arcrad=arcrad+st_sht
```

```
        x_pol(2,6)=st_wid/4.0d0
        y_pol(2,6)=((arcrad)**2.0d0-(x_pol(2,6))**2.0d0)**0.5d0
        x_pol(2,13)= 0.0d0
        y_pol(2,13)= st_id/2.0d0+st_sht
        call drecpol( x_pol(2,13),y_pol(2,13),rr,ap1)
        call drecpol( x_pol(2,6),y_pol(2,6),rr,ap2)
        ainc=(ap1-ap2)/7.0d0

        do i=13,6,-1
        call dpolrec(arcrad,ap1-ainc*dble(13-i),arc_x,arc_y)
        x_pol(2,i)=arc_x+aoff_x
        y_pol(2,i)=arc_y+aoff_y
        end do

c points for region 3:

        arcrad=st_id/2.0d0
        x_pol(3,1)=-st_wid/2.0d0
        y_pol(3,1)=((arcrad)**2.0d0-(x_pol(3,1))**2.0d0)**0.5d0
        x_pol(3,5)=x_pol(1,1)
        y_pol(3,5)=y_pol(1,1)
        call drecpol( x_pol(3,1),y_pol(3,1),rr,ap1)
        call drecpol( x_pol(3,5),y_pol(3,5),rr,ap2)
        ainc=(ap1-ap2)/4.0d0

        do i=1,5
        call dpolrec(arcrad,(ap1-ainc*dble(i-1)),arc_x,arc_y)
        x_pol(3,i)=arc_x+aoff_x
        y_pol(3,i)=arc_y+aoff_y
        end do

        arcrad=st_id/2.0d0+st_sht
```

```
        x_pol(3,9)=-st_wid/2.0d0
        y_pol(3,9)=((arcrad)**2.0d0-(x_pol(3,9))**2.0d0)**0.5d0
        x_pol(3,6)= x_pol(1,13)
        y_pol(3,6)= y_pol(1,13)
        call drecpol( x_pol(3,9),y_pol(3,9),rr,ap1)
        call drecpol( x_pol(3,6),y_pol(3,6),rr,ap2)
        arcang10=ap1
        ainc=(ap1-ap2)/3.0d0

        do i=9,6,-1
        call dpolrec(arcrad,(ap1-ainc*dble(9-i)),arc_x,arc_y)
        x_pol(3,i)=arc_x+aoff_x
        y_pol(3,i)=arc_y+aoff_y
        end do

        x_pol(3,11)= (x_pol(3,1)+x_pol(3,9))/2.0d0
        y_pol(3,11)= (y_pol(3,1)+y_pol(3,9))/2.0d0
        x_pol(3,10)= (x_pol(3,9)+x_pol(3,11))/2.0d0
        y_pol(3,10)= (y_pol(3,9)+y_pol(3,11))/2.0d0
        x_pol(3,12)= (x_pol(3,1)+x_pol(3,11))/2.0d0
        y_pol(3,12)= (y_pol(3,1)+y_pol(3,11))/2.0d0


c points for region 4-23 are not shown here
c points for region 24

        arcrad= st_od/2.0d0
        arcang= (pi/2.0d0)-(spitch/2.0d0)
        call dpolrec(arcrad,arcang,arc_x,arc_y)
        x_pol(24,5)= arc_x
        y_pol(24,5)= arc_y
```

```
        do i=1,3
        x_pol(24,i)= x_pol(20,(8-i))
        y_pol(24,i)= y_pol(20,(8-i))
        end do

        x_pol(24,7)= x_pol(22,6)
        y_pol(24,7)= y_pol(22,6)
        x_pol(24,8)= x_pol(22,5)
        y_pol(24,8)= y_pol(22,5)
        x_pol(24,6)= 0.5d0*(x_pol(24,5)+x_pol(24,7))
        y_pol(24,6)= ((arcrad)**2.0d0-(x_pol(24,6))**2.0d0)**0.5d0
        x_pol(24,4)= 0.5d0*(x_pol(24,3)+x_pol(24,5))
        y_pol(24,4)= 0.5d0*(y_pol(24,3)+y_pol(24,5))

        return
        end
c end of sub stator_slot_1
c -------------------------------------------------
c      sub drecpol converts rectangular to polar
        subroutine drecpol(x,y,r,theta)
        double precision x,y,r,theta,pi,tol
        pi=2.0d0*dasin(1.0d0)
        tol=pi/1.0d8
        r=(x*x + y*y) **(0.5d0)
              if (x .ne. 0.0 ) then
                theta=datan2(y,x)
           if ((theta.gt.(-pi-tol)).and.
     +         (theta.lt.(-pi+tol))) then
                theta=pi
          end if
              else
                if (y .lt. 0.0) theta=3.0d0*pi/2.0d0
```

```
                if (y .gt. 0.0) theta=pi/2.0d0
              end if
        return
        end
c end of sub drecpol
c -------------------------------------------------
c      sub dpolrec converts polar to rectangular
        subroutine dpolrec(r,theta,x,y)
        double precision r ,theta, x, y
        x=r*dcos(theta)
        y=r*dsin(theta)
        return
        end
c end of sub drecpol
c -------------------------------------------------
c       Function degrad converts degrees to radians
        function degrad(Theta)
        double precision theta,pi,degrad,tmp
        tmp=1.0
        pi=2.*dasin(tmp)
        DEGRAD = theta /180.0 * pi
        return
        end
c end of function degrad
c -------------------------------------------------
c       Function FIM converts inches to metres
        function fim(an_inch)
        double precision an_inch,fim
        fim=an_inch*0.0254d0
        end
c end of function degrad
c -------------------------------------------------
```

Appendix B

Program for mesh generation and solver

```
c solve.f.nw
c for a SWITCHED RELUCTANCE MACHINE
c       (c) af volschenk, 1994
c       contact: MJ Kamper, Dept e/e Eng, Stellenbosch, 7600
c       tel:021-8084481
c       revision history
c       13 October 1998
c       design optimisation
c-----------------------------------------------------------------
c
c variable declarations
c
      SUBROUTINE eesolv(xpar,ypar)
c ----------------------------------------------------------------
      open (22,file="results/performb.res", form='formatted')
      rewind 22
      write(22,103)
      write(22,151)
      write(22,103)
  103 format('')
  131 format(11F8.2)
```

```
  151 format('Start 11/12/98:Perform:340/175; Optimum dimensions')
c ---------------------------------------------------------------------
      pi=4.0d0*datan(1.0d0)
      sqrt2=dsqrt(2.0d0)
      sqrt3=dsqrt(3.0d0)

c  ------------------------------------------------
c          INPUT ROTOR AND STATOR PARAMETERS
c  ------------------------------------------------
c
      st_wid=xpar(1)*0.001d0
      st_id=xpar(2)*0.001d0
      st_yh=xpar(3)*0.001d0
      ro_tw=xpar(4)*0.001d0
c -->
        st_id=0.192628009d0
        airg_l=0.00062d0
        ro_od=st_id-2.0d0*airg_l
c the other rotor pole dimensions stay the same:
         n_ro_st=2
c -->
         ro_tw=0.060d0
         ro_yh=0.5d0*ro_tw
         ro_shfd=0.07d0
         ro_th=(ro_od-ro_shfd-2.0d0*ro_yh)/2.0d0
         ro_flr=0.004d0
c
c and save to data file
c
        rs_file='mjk_nbr.dat'
        rs_type='fbr'
        call save_rslot(rs_file,rs_type,ro_od, n_ro_st,ro_shfd,ro_ang,ro_flr,
```

```
     &    ro_yh,ro_th,ro_tw)
c  ---------------------------------------------------
c         INPUT STATOR PARAMETERS
c  ---------------------------------------------------
c
        ss_type='sss'
        n_st_st=6
c -->
        st_od=0.34d0
        st_yh=0.0310210581d0
        st_slh=(st_od-st_id)/2.0d0-st_yh
        st_sht=0.12d0*st_slh
        st_shs=0.440d0*st_slh
        st_shb=0.440d0*st_slh

c -->

c calculate further (pp.2):
        a_slt=dble(n_st_st)
        spitch1= (2.0d0*pi*(st_id/2.0d0+st_sht))/(a_slt)
        st_wid= 0.0549576964d0
        st_twg= 0.035d0*spitch1
        st_wbw= st_twg
        spitch= (pi*st_id)/(a_slt)
        st_wag= st_wbw

c other parameters:
        stack=0.97d0
        f=50.0
        v_line=380.0
        temp=100.0
        fill_f=0.75
```

```
c -->
        w=0.175d0*stack
        p_cu=1500.0d0
        p_wf=300.0d0
        l_ce=0.27d0
c
c and save to data file

        ss_file='mjk_ss1.dat'
        call save_sslot(ss_file,ss_type,n_st_st, st_od,st_id,st_gw,st_waw,st_wag,st_bw,
     &    st_wid,st_twg,st_sht,st_shs,st_shb,st_wbw,st_yh,spitch,st_slh)

c       goto 133

c  ----------------------------------------------------
c       MAKE THE MESH AND START WITH CALCULATIONS
c  ----------------------------------------------------
c
        ofile='temp/mjk2.pol'
        ifile='mjk2.fpl'
        def_file='mjk2.def'

c make the mesh and save to mjk2.fpl
c
        CALL ee_as(def_file,ofile,rat)
        CALL ee_pmesh(ofile,ifile,nelm,nnode)
c
c and then do the preprocessing
c
        CALL ee_pre(def_file,nprof)
c Files for solver
```

```
c
c now read a fewe more defaults
c main mesh info
c
        call sreadmesh(fname,nde,nelm,nnode,x,y,node,itype, testa,nlines,line,neigh)
c
c winding info
c
        call read_sw(w_file,n_st_sp,nw_it,nw_f,nw_t, nw_ci,wn,rw,end_w,ns)
c convert the X_end-winding to inductance
c calculate l_end separately
c
c stator slots etc
c
c number of poles
        np = 2
c number of pole pairs
        nppole=np/2
c number of stator slots per pole
        nslots=n_st_rq
c number of stator slots per pole per phase
        ns_pph=nslots/ns
c number of pole pitches in model
        npp=n_st_rq/n_st_sp
c
c---------------------------------------------------------------
c
c program main body
c
c ---------------------------------------------------------------

c pole-pitch?
```

```
        p_pitch=dble(1/6)*2.0d0*pi
c synchronous speed electrical radians
        omegas=f*pi*2.0d0
        s_speed=60.0d0*f/nppole

c circuit numbering convention
c       phase a 1
c       phase b 2
c       phase c 3
c
        do i=1,ns
          acoil(i)=scoil(i)/2.0d0/ns_pph
        end do
c
c -->   nc_turns
        nc_turns(1)=56

c -->   Always 1 for the SRM
        np_cir=1

c Number of windings in series per phase: SRM
        nphase=nc_turns(1)*2.0d0

c Calculate the per phase stator resistance at 100 deg.C
        a_cu=acoil(1)*0.82d0
c Make it simple
        a_sc=0.5d0*acoil(1)/nc_turns(1)
        r_s=nphase*17.0d-9*1.31d0*(w/stack+l_ce)/a_sc
c ***************************************************************
c  PROGRAM: Calculate flux linkages
c ***************************************************************
c
        open(39,file="results/taprdtok.res",form='formatted')
```

```
      rewind 39
      write(39,390)
      write(39,392)
      Tmin=2000.0d0
      Tsum=0
      it=0
      c_cur(1)=0.0d0
      c_cur(2)=0.0d0
      c_cur(3)=0.0d0
      do mem=2,2
        alpha=0.0d0

c
c For the SRM: activated for flux/current calculations
        do icurrent=30,30
          c_peak=(sqrt3*dsqrt(p_cu/r_s/3.0d0))
         c_cur(1)=0.0d0
          c_cur(2)=c_peak
          c_cur(3)=0.0d0
c
          cur(1)=c_cur(1)
          cur(2)=c_cur(2)
          cur(3)=c_cur(3)

          th_off=-15.0d0*pi/180.0d0
          step_angl=1.0d0*pi/180.0d0
          do angl=0,0
            it=it+1
            if(mem.eq.1) ithet_m=angl
            if(mem.eq.2) ithet_m=angl+30
            if(mem.eq.3) ithet_m=angl+60
            theta_m=dble(ithet_m)*pi/180.0d0
```

```
              theta(it)=dble(ithet_m)

c       print *,'--------------------------------------'
c
c calculate torque:change 100 to lesser values

       call torque(rrad,srad,torq1,50,nppole,nrs,nraz, ax,a,an,bn,razind)
       torquei(it)=torq1
       Tsum=Tsum+torq1
       if (torquei(it).lt.Tmin) Tmin=torquei(it)
       write(39,291) torquei(it)
       end do

c end of ithet_m
c calculate average torque

       Tave=Tsum/it

       open (20,file="DATA/Tmin1.dat", form='formatted')
       rewind 20
       write(99,290)
       write(99,292)
       do 25 it=1,90,1
         write(20,291) torquei(it)
    25 continue
       write(20,290)
       close(20,status='keep')

   290 format('')
   291 format(f15.6)
   292 format('Start 03/12/98:T from 4 rotor positions: phase2')

c ====================================================
```

```
c       FINAL CALCULATIONS
C ======================================================


c Some more calculations
c ---------------------------------------
      i_rms= c_peak*dsqrt(1.0d0/3.0d0)
      T_out= Tef-p_wf*dble(nppole)/omegas
      p_cu=3.0d0*r_s*i_rms**2
      p_in=kva*p_fact*1000.0d0
      cur_den=i_rms/(a_sc*1.0d+6)
c
c --------------------------
c results to main program
c --------------------------

      Tr=640.0d0
      pry=10500.0d0

      ypar(1)=c_peak
      ypar(2)=0.0d0
      ypar(3)=cur_den
      ypar(4)=Tave
      ypar(5)=0.0d0
      ypar(6)=0.0d0
      ypar(7)=p_cu/1000.0d0
      ypar(8)=0.0d0
      ypar(9)=0.0d0
      ypar(10)=0.0d0
      ypar(11)=0.0d0

c write to file:performb.res
```

```
      write(22,103)
      write(22,131) ypar(1),ypar(2),ypar(3),ypar(4),ypar(5),ypar(6),
     &  ypar(7),ypar(8),ypar(9),ypar(10),ypar(11)

c       end do
c end of rotate ithet_m

c       end do
c end of alpha
      it=0
      end do
c end of mem
      end do
c end of icurrent
      close (22,status='keep')
      close (39,status='keep')
-----------------------------------------------------------------------
```

Appendix C

The prototype SRM

The diagrams shown here are for the prototype of the tapered stator pole SRM. This is the machine that was built and used in verifying the FEM calculated results. In these diagrams only the essential parts of the machine are shown, i.e. the stator, the rotor and the stator windings.

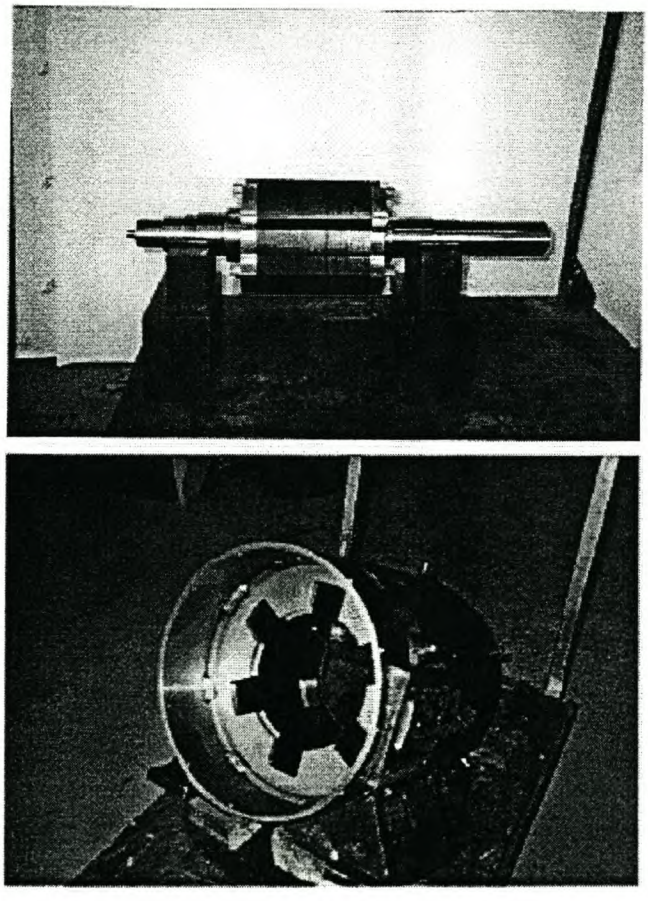

Figure C.1: **The rotor and the stator of the prototype SRM machine**

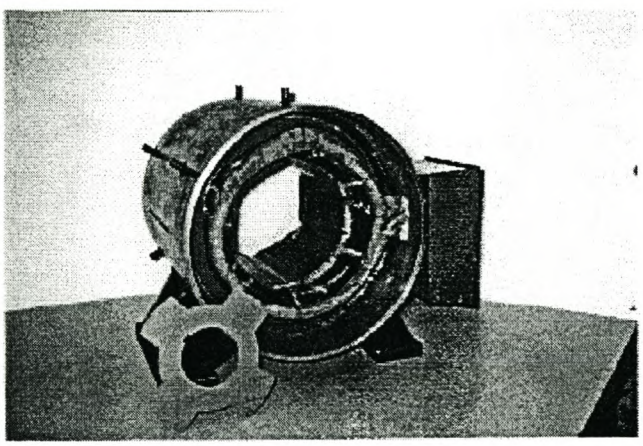

Figure C.2: **The figure shows stator windings of the prototype machine and a lamination of the rotor in front of the machine**

Appendix D

Test setup

The test machine shown in Fig. D.1 shows the actual bracket-loadcell setup that was used in the static torque measurements. Also the figure shows the complete SRM with the terminal box.

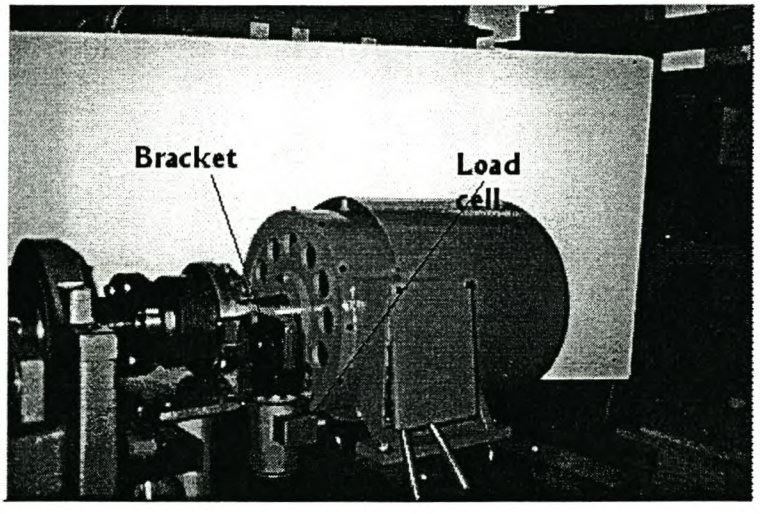

Figure D.1: **The picture shows test setup with bracket and load cell indicated**

Bibliography

[1] Martyn R.Harris, John W.A.Mallick, Timothy J.E.Miller, "A review of the integral-horsepower switched reluctance motor drive", IEEE Transactions on Industry Applications, Vol. 1A-22, No.4, July/August 1986, pp 716-721.

[2] J. Reed, "Switched reluctance drive systems", Proceedings of the conference on Drives/Motors/Controls '83, Horrogate, UK, 12th-14th October 1983, pp. 118-121.

[3] C.Neagoe, A.Foggia and R.Krishnan, "Impact of pole tapering on the electromagnetic torque of the switched reluctance motor", IEEE International Electric machines and Drives Conference Record, IEMDC 1997, pp. WA1 2.1-2.3.

[4] J-Y Le Chenadec, M.Geoffroy, B.Multon and J-C Mouchoux, "Torque ripple minimisation in switched reluctance motors by optimisation of current wave-forms and of tooth shape with copper losses and "V.A. Silicon" constaints", ICEM 94, p.559-64, Vol.3.

[5] R.Arumugam, J.F.Lindsay and R.Krishnan, "A comparison of the performance of two different types of switched reluctance motors". Electric Machines and Power Systems, 12: p.281-7, 1987.

[6] J.W.Finch, M.R.Harris, A.Musoke and H.M.B.Metwally, "Variable speed drives using multi-teeth per pole switched reluctance motor", Proc. 13th Annual Symposium on Incremental Motion Control System and Devices, May 1984, p. 293-301.

[7] T.J.E.Miller, "Brushless permanent-magnet and reluctance motor drives", Clarendon Press, Oxford, 1989, Ch. 7.

[8] P.J.Lawrenson, J.M.Stephenson, P.T.Blenkinskop, J.Corda, N.N.Fulton, "Variable-speed switched reluctance motors", IEE Proc., Vol. 127, Pt.. B, No. 4, July 1980, p.253-265.

[9] Slobodan Vukosavic/ and Victor Stefanovic/, "SRM inverter topologies: A comparative evaluation", IEEE Transactions on Industry Applications, Vol.27, No.6, Nov/Dec 1991, p.1034-1047.

[10] W.F.Ray, P.J.Lawrenson, R.M.Davis, J.M.Stephenson, N.N.Fulton, R.J.Blake, "High-performance switched reluctance brushless drives", IEEE Transactions on Industry Applications, Vol.1A-22, No.4, Jul/Aug 1986, p.722-730.

[11] T.J.E.Miller, P.G.Bower, R.Becerra, M.Ehsani, "Four-quadrant brushless reluctance motor drive", Third International Conference on Power Electronics and Variable -Speed Drives, July 1988, p.273-6.

[12] J.Faiz, J.W.Finch, "Aspects of design optimisation for switched reluctance motors", IEEE Transactions on Energy Conversion, Vol.8, No.4, December 1993, pp. 704-713.

[13] F.Sahin, H.B.Ertan, K.Leblebicioglu, "Optimum geometry for torque ripple minimisation of switched reluctance motors", International Journal for Computation and Mathematics in Electrical and Electronic Engineering (COMPEL), Vol. 14, No.4, Dec 1995, pp. 117-121.

[14] M.R.Harris, A.Hughes, P.J.Lawrenson, "Static torque production in saturated doubly-salient machines", IEE Proc., Vol.122, No.10, October 1975, pp.1121-1127.

[15] Jacek F.Gieras, Mitchell Wing, "Permanent motor technology: Design and Applications", Marcel Dekker, Inc., 1997.

[16] M.J.Kamper, "Design Optimisation of Cageless Flux Barrier Rotor Reluctance Synchronous Machine", Ph.D. dissertation, University of Stellenbosch, 1996.

[17] M.J.D.Powell, "An efficient method for finding the minimum of a function of several variables without calculating derivatives", Computer Journal, Vol.7, pp. 155-162, 1964.

[18] M.J.Kamper, F.S.van der Merwe, S.Williamson, "Direct finite element design optimisation of the cageless reluctance synchronous machine", IEEE Transactions on Energy Conversion, Vol. 11, No. 3, September 1996, pp. 547-553.

[19] A.E.Fitzgerald, C.Kingley Jr, S.D.Umans, "Electric Machinery", McGraw-Hill., Inc, 1990.

[20] A.F.Volschenk, "Finite element analysis of a salient-pole generator feeding a rectifier load", Ph.D. dissertation, University of Cambridge, March 1993.

[21] T.J.Flack, A.F.Volschenk, "Computational aspects of time-stepping finite-element analysis using an airgap element", ICEM, Sept 1994.

[22] A.A.Abdel-Razek, J.L.Coulomb, J.C.Sabonnadiere, "Conception of an air-gap element for the dynamic analysis of the electromagnetic field in electric machines", IEEE Transactions on magnetics, Vol. 18, No. 2, Mach 1982, pp. 655-659.